JBC Papers in Press. Published on March 9, 2005 as Manuscript M500809200

Biochemical and Biophysical Characterization of Photosystem I from Phytoene Desaturase and Zeta-carotene Desaturase Deletion Mutants of *Synechocystis* sp. PCC 6803: Evidence for PsaA- and PsaB-Side Electron Transport in Cyanobacteria†

James A. Bautista[1‡], Fabrice Rappaport[2‡], Mariana Guergova-Kuras[2], Rachel O. Cohen[3], John H. Golbeck[3,4], Jamie Yehong Wang[1], Daniel Béal[2] and Bruce A. Diner[1,*]

Running title: Carotenoids sense PsaA- and PsaB-side electron transport

From [1] CR&D, Experimental Station, E. I. du Pont de Nemours & Co., Wilmington, DE 19880-0173 U. S. A. [2] UMR 7141 CNRS/Univ. Paris 6, Institut de Biologie Physico-Chimique, 13 rue Pierre et Marie Curie, 75005 Paris, FRANCE [3] Department of Biochemistry and Molecular Biology, The Pennsylvania State University, University Park, PA 16802 U. S. A. [4] Department of Chemistry, The Pennsylvania State University, University Park, PA 16802 U. S. A

Address correspondence to: Bruce A. Diner, CR&D, Experimental Station, E. I. du Pont de Nemours & Co., Wilmington, DE 19880-0173, Tel. 302 695-2494, Fax. 302 695-9183; E-mail: bruce.a.diner@usa.dupont.com

In Photosystem I, oxidation of reduced acceptor A_1^- through iron-sulfur cluster F_X is biphasic with half times of ~5-30 ns ("fast" phase) and ~150-300 ns ("slow" phase). Whether these biphasic kinetics reflect unidirectional electron transfer, involving only the PsaA-side phylloquinone or bi-directional electron transfer, involving both the PsaA- and PsaB-side phylloquinones, has been the source of some controversy. Brettel (*FEBS Lett.* 239, 93-98) and Joliot and Joliot (*Biochemistry* 38, 11130-11136) have attributed to nearby carotenoids electrochromic band shifts, accompanying A_1 reduction, centered at ~450 nm and 500-510 nm. As a test of these assignments, we separately deleted in *Synechocystis* sp. **PCC 6803 the genes that encode Pds and Zds (*crtP* (*pds*) and *crtQ* (*zds*), respectively). The *pds*$^-$ and *zds*$^-$ strains synthesize phytoene and zeta-carotene, respectively, both of which absorb to shorter wavelength than β-carotene. Compared to WT, the mutant A_1^-(FeS) - A_1(FeS)$^-$ difference spectra, measured in cells and PS I complexes, retain the electrochromic band shift centered at 450 nm but show a complete loss of the electrochromic band shifts centered at 500-510 nm. Thus, the latter clearly arise from β-carotene. In the WT, the electrochromic band shift of the slow phase (centered at 500 nm) is shifted by 6 nm to the blue compared to the fast phase (centered at 506 nm). Thus, the carotenoid pigments acting as electrochromic markers during the fast and slow phases of A_1^- oxidation are different, indicating the involvement of both the PsaA- and the PsaB-side phylloquinones in PS I electron transport.**

The Photosystem I (PS I) reaction center is a multisubunit intrinsic membrane protein complex that functions as a light-driven plastocyanin/ferredoxin oxidoreductase. At the core of PS I is a heterodimer of two highly homologous subunits, PsaA and PsaB, which contain the redox components involved in the first steps of photoinduced electron transfer. Light energy initiates primary electron transfer such that the oxidizing equivalent resides on P700, a heterodimer of chlorophyll *a* (Chl *a*) and its C13^2-epimer Chl *a*' (1-3). In chronological order, the electron acceptors are: A_0 (Chl *a*), A_1 (phylloquinone or Vitamin K_1), F_X (a [4Fe-4S] cluster) and the terminal electron acceptors F_A and F_B (both [4Fe-4S] clusters). All are bound by PsaA and PsaB except for F_A and F_B, which are bound to subunit PsaC. The PS I complex also includes two additional small extrinsic polypeptides, PsaD and PsaE, which mediate the docking of ferredoxin (4), the soluble electron carrier responsible for the reduction of $NADP^+$, and PsaF which facilitates the binding of plastocyanin, the mobile electron carrier responsible for the re-reduction of the oxidized donor, $P700^+$ (5-7).

In addition to these redox cofactors, carotenoids and other Chl *a*'s are also bound within the PS I complex. A 2.5 Å X-ray crystallographic structure of the trimeric PS I reaction center from the thermophilic cyanobacterium *Thermosynechococcus elongatus* was recently reported (2). Resolved in each monomer of the crystal structure were 22 carotenoids, 96 chlorophylls *a*, 2 phylloquinones, and 3 [4Fe-4S] clusters. The two phylloquinone molecules are symmetrically located with respect to the C_2 symmetry axis of the protein heterodimer. Whether the PsaB-side quinone as well as the PsaA-side quinone are active for electron transfer has been the subject of considerable recent debate. Optical studies have shown that the reoxidation of A_1^- is biphasic ($t_{1/2}$ of 5-30 ns and 150-300 ns) (8,9) but the assignments and interpretations of these two kinetic phases are still controversial (10). To explain the biphasic kinetics, Brettel (8,10,11) originally proposed a model where rapid equilibration between A_1 and F_X would give rise to the faster phase of A_1^- reoxidation while the depletion of this quasi-equilibrium by electron transfer to F_A/F_B would give rise to the slower phase. The same phylloquinone was proposed to participate in both phases. Joliot and Joliot (12) showed, however, that the relative amplitudes of the fast and slow phases were insensitive to the membrane potential, inconsistent with the attribution of the fast phase to the formation of equilibrated state, $A_1^-F_X \rightleftarrows A_1F_X^-$, an electrogenic electron transfer step (13). They suggested that the biphasic kinetics could come from either of two models: (i) a single phylloquinone molecule in two different conformational states having different A_1^- reoxidation rates or (ii) two different phylloquinones, one on each side of the reaction center and oxidized by F_X at different rates. The former would constitute a unidirectional pathway while the latter would be bidirectional. The X-ray structure reveals no obvious differences between the binding pockets of the two phylloquinones nor a difference in the phylloquinone-F_X edge-to-edge distances (6.8 Å). Recently, Guergova-Kuras et al. (14), using site directed mutants of *C. reindhardtii*, provided the first experimental support for the participation of both the PsaA-side and PsaB-side quinones in electron transfer to F_X. Site directed replacement of the tryptophan directly π-stacked to the PsaA-side phylloquinone with phenylalanine (PsaA-W693F), selectively slowed the slower phase of A_1^- reoxidation while the same mutation of the corresponding tryptophan on the PsaB-side (PsaB-W673F) selectively slowed the faster phase. Xu and coworkers (10) using the cyanobacterium *Synechocystis* sp. PCC 6803, confirmed the room temperature optical results on the PsaA-W693F and the PsaB-W673F mutations, but while transient EPR studies provided experimental evidence for PsaA-side electron transfer , there was no indication of PsaB-side electron transfer. Similarly, Cohen et al. (15) constructed site-directed mutants in which the axial methionine ligands to chlorophylls eC-A_3 and eC-B_3 were changed to leucine, and found an effect on the transient EPR signal only on the PsaA-side mutant. They concluded that electron-transfer occurs primarily along the PsaA-branch in cyanobacteria, although a minor fraction of electron transfer along the PsaB-branch could not be excluded. Fairclough and coworkers (16), however, constructed a site-directed replacement with histidine of a methionine ligand to chlorophyll eC-A_3 in *C. reindhardtii*, PsaA-M684H, that still allows photoautotrophic growth despite having blocked electron transfer to the PsaA-branch phylloquinone. This observation implies that the PsaB-branch is active for electron transfer and that its activity is sufficient to support photoautotrophic growth. This mutation and the corresponding PsaB-side ligand replacement, PsaB-M664H, were constructed by Fairclough et al (16) and by Ramesh and coworkers (17). Both mutations block or slow electron transfer from A_0^- to A_1 on their respective branches, implying that in *C. reindhardtii* both PsaA- and PsaB- branches are active in electron transport.

All of the carotenoids in the electron density map derived from the X-ray crystal structure of PS I were modeled as β-carotene (2). Seventeen were in an all-*trans* configuration. Two were modeled as 9-*cis*, another showed a 13-*cis* configuration, and two were shown with 2-*cis* double bonds: 9,9'-di*cis,* and 9,13'-di*cis*. (for numbering, see Fig. 1 and ref. (18)). The carotenoids are arranged in six clusters with each cluster containing 2, 3 or 6 carotenoids. (See Fig. 9 of ref. (3).) In cyanobacteria and in other carotenoid-producing organisms, carotenoids are

synthesized from isoprenoid precursors. The first step specific for carotenoid biosynthesis is the head-to-head-condensation of geranylgeranyl pyrophosphate (See Fig. 1). This reaction is catalyzed by phytoene synthase and forms phytoene, a C_{40} carotenoid with 3 conjugated double bonds. Phytoene desaturase (encoded by *crtP* (*pds*)) catalyzes the double dehydrogenation of phytoene to form zeta-carotene, which possesses 7 conjugated double bonds. Another enzyme, zeta-carotene desaturase (encoded by *crtQ* (*zds*)), is responsible for the dehydrogenation of zeta-carotene to form lycopene, a carotenoid with 11 conjugated double bonds. Lycopene cyclase catalyzes the formation of β-ionylidene rings at both ends of lycopene to form β-carotene, still with 11 conjugated double bonds but with the terminal double bonds being part of the rings. β-carotene can then be hydroxylated in the rings by specific β-carotene hydroxylases to form β-cryptoxanthin, isocryptoxanthin and/or zeaxanthin (Fig. 1).

Brettel (11) and Joliot and Joliot (12) proposed that the reduction of the PS I phylloquinone electron acceptor, A_1, produces electrochromic band shifts centered at 450 and 500-510 nm of one or more nearby carotenoid molecules. According to the x-ray crystal structure, several carotenoids with different orientations and configurations and modeled as β-carotene, are indeed present in the immediate vicinity of each of the two phylloquinone molecules. If both branches of the electron transport chain were active, then each of the phylloquinones should show electrochromic shifts of two different sets of carotenoids, the absorption spectra of which might be slightly different. To examine this possibility, we have altered the carotenoid biosynthetic pathway to replace β-carotene with carotenoids having shorter π– conjugation, the absorbance bands of which are blue-shifted compared to β-carotene. This replacement should shift the carotenoid electrochromism to shorter wavelengths allowing the WT carotenoid band shifts associated with A_1^- formation to be clearly identified.

The results presented here show that associated with each of the two phases of the A_1^- reoxidation is the loss of electrochromic band shifts on two different sets of carotenoid molecules with different absorbance spectra. These spectral differences are consistent with the differences in configuration of the carotenoids close to phylloquinones on the PsaA- and PsaB-branches as seen in the X-ray crystal structure. These results support therefore a model for electron transport in PS I in which both the PsaA- and PsaB-side phylloquinones participate in electron transfer to F_X.

Materials and Methods

Construction of Mutants - The genes for phytoene desaturase (*pds*) and zeta-carotene desaturase (*zds*) were deleted separately in the genome of wild type (WT) *Synechocystis* sp. PCC 6803 and replaced by a kanamycin resistance cassette. A PCR copy of the gene to be deleted (*pds* or *zds*) that included 500 bases upstream and downstream of the gene was ligated onto a pGEM-T plasmid vector (Promega A1360) using T4 DNA ligase and amplified in XL1-Blue *E. coli* competent cells (Stratagene 200249). In this resulting plasmid, the first and last 50 bases of the gene together with the ligated pGEM-T plasmid vector between them were copied by PCR using primers designed to give unique restriction enzyme sites to the termini of the PCR product. The PCR product was digested with the appropriate restriction enzymes and then ligated using T4 DNA ligase to a kanamycin resistance cassette with the same sticky ends as the PCR product. This final plasmid construct was then amplified in XL1-Blue *E. coli* competent cells and used to transform the WT *Synechocystis* sp. PCC 6803 strain. Transformation of *Synechocystis* sp. PCC 6803 WT strain was as described in Nixon et al (19). Successful transformants were selected on Petri plates containing BG-11 medium, 5 mM glucose, 50 μg/mL kanamycin and grown in very dim light (~0.1 umol photons $m^{-2}s^{-1}$) at 30° C. Kanamycin-resistant colonies representing successful transformants were replated 7 times in BG-11 plates containing 5 mM glucose and 200 μg/mL kanamycin to obtain full segregation. Deletion mutations were confirmed by extracting total pigments from the cells and analyzing for the complete absence of β-carotene by HPLC (see below). The cells were also unable to produce β-

carotene under non-selective conditions (without kanamycin).

PS I Preparation - WT *Synechocystis* sp. PCC 6803 cells were grown in liquid BG-11 containing 5 mM glucose medium as described (20-22). The mutants were grown in BG-11 containing 5 mM glucose in very dim light (~0.1 umol photons $m^{-2}s^{-1}$). Isolation of the thylakoid membranes from these cells was performed as previously described (20,21). The thylakoid membranes were suspended at a concentration of 1 mg/mL chlorophyll in Buffer A (25% glycerol, 20 mM $CaCl_2$, 5 mM $MgCl_2$, 50 mM MES pH 6.0). After addition of a one-ninth volume of 10% (w/v) *n*-dodecyl-β-D-maltoside (β-DM) (final concentration of 1% (w/v)) the suspension was stirred for 20 min and then centrifuged at 55,000 rpm in a 70Ti rotor (Beckman-Coulter) for 30 min. The supernatant was then loaded onto a ~ 500 mL weak-anion exchange Toyopearl DEAE-650S (Supelco) column pre-equilibrated with Buffer B (Buffer A containing 0.03% β-DM) and washed with Buffer B containing 19 mM $MgSO_4$. Elution of PS I complex from the column was performed using 500 mL Buffer B, forming an increasing salt gradient from 19 to 30 mM $MgSO_4$. At the end of the gradient the salt concentration was increased to 50 mM $MgSO_4$. The eluent fractions containing PS I were pooled and concentrated in a Millipore concentrator utilizing a YM 100 Diaflo ultrafiltration membrane. The concentrated samples were then desalted by passing them through a gel filtration column (Econo-Pac 10 DG, Bio-Rad) pre-equilibrated with Buffer B. The samples were then frozen in liquid N_2, and stored at -80^{o} C until use.

Pigment analysis - The chlorophyll content of the cells was determined by extraction with 100% methanol and using the 79.24 mL/mg extinction coefficient of Lichtenthaler (23) at 665 nm. For total pigment analysis, PS I complexes were extracted with a 50:50 acetone/methanol mixture under dim light. The mixture was centrifuged for 2 min (10,000 x g) and a 50 μL aliquot of the supernatant was immediately filtered (0.45 μm, Millex-LH PTFE) and injected onto a reverse-phase HPLC column (Zorbax-ODS, 4.6 mm x 15 cm, Rockland Technologies) equilibrated with methanol:ethyl acetate (68:32, v/v). The separation was performed in isocratic mode using the same solvent system (24) at a flow rate of 0.25 mL/min for 60 min at room temperature. The relative chlorophyll and carotenoid concentrations were determined by measuring the area of their respective peaks in the HPLC chromatogram and dividing by the extinction coefficients according to Giorgi *et al.* (24).

EPR Spectroscopy - X-band (9.4 GHz) EPR studies were performed using a Bruker ECS-106 spectrometer and a standard-mode resonator (ST 8615) equipped with a slotted port for light entry. Cryogenic temperatures were maintained with a liquid helium cryostat and an ITC-4 temperature controller (Oxford UK). The microwave frequency was measured with a Hewlett-Packard 5340A frequency counter and the magnetic field was calibrated using α,α'-diphenyl-β-picryl hydrazyl as the standard. Sample temperatures were monitored by a calibrated thermocouple located 3 mm beneath the bottom of the quartz sample tube and referenced to liquid N_2. The spectra of F_A^-/F_B^- in WT and mutant PS I complexes were obtained as previously described (25). Glycine buffer (1 M) was added to bring the pH to 10.0 (100 mM final concentration) and sodium dithionite was added to a final concentration of 50 mM. The sample was incubated in darkness on ice for 30 min, after which the sample was frozen in liquid N_2 and the EPR spectrum was recorded at 15K.

Q-band (34 GHz) EPR studies were performed using a Bruker ER 5106 QT-W1 resonator equipped with a port for sample illumination. Cryogenic temperatures were maintained with a Bruker ER4118CV liquid nitrogen cryostat and a Bruker ER4121 temperature control unit. The microwave frequency was measured with a Bruker ER035M NMR gaussmeter. The magnetic field was calibrated with γ,γ-bisdiphenylene-β-phenylallyl (BDPA) complexed 1:1 with benzene which has no detectable g-anisotropy at 34 GHz. Photoaccumulation of A_1^- and F_X^- in all PS I samples was carried out as described in ref. (26). The pH of the sample was adjusted to 10.0 with glycine buffer (1 M) (final concentration of 100 mM) and sodium dithionite was added to a final concentration of 50 mM. After incubation for 20 min in the dark on ice, the sample was frozen in

liquid nitrogen and placed in the microwave cavity. A pre-illumination spectrum was then recorded at 205 K. The sample was then illuminated with a 20 mW He-Ne laser for 40 min at 205 K. The laser was then turned off, and the light-induced spectrum was recorded at the same temperature. The light-minus-dark difference spectrum at 205 K shows primarily A_1^-, as signals from F_X^- and the other iron-sulfur clusters are only detectable at very low temperatures (less than 20K).

Optical spectroscopy - Charge recombination kinetics from F_A^-/F_B^- to $P700^+$ nm were measured at 435 nm in a laboratory-built flash-detection spectrophotomer similar to that originally described by Joliot et al. (27). PS I complexes at a Chl *a* concentration of 14 μg/mL were suspended in 25 mM Tris-HCl (pH 8.3), 10 μM sodium ascorbate plus 4 μM DCPIP (or 250 μM sodium ascorbate without DCPIP), and 0.03% β-DM. Under these conditions, P700 is fully reduced and all electron acceptors are oxidized prior to excitation (26). Charge separation was induced by a saturating flash (30 mJ) provided by a linear flash lamp pulsed dye laser (Model LFDL-3, Cynosure Inc.) using Rhodamine 590 perchlorate (Exciton). The reduction of $P700^+$ by recombination was measured at 435 nm using detecting flashes provided by an EG&G FX199U flash lamp and passed through a Jobin-Yvon HL300 monochromator.

Measurements of the kinetics of A_1^- oxidation in the nanosecond to microsecond time scale were performed on whole cells and isolated PS I complexes in a flash-detection spectrophotometer previously described (14,28). Whole cells were suspended in 20 mM HEPES (pH 7.2), 20% (w/v) Ficoll, and 5 μM FCCP. The PS I complexes were suspended at a concentration of 40 μg/mL under the same conditions as for charge recombination, except that the sodium ascorbate and DCPIP concentrations were 10 mM and 40 μM, respectively. Decay-associated spectra of the kinetic phases were derived from a global multi-exponential fit of the kinetic components obtained at each wavelength, using the program MEXFIT (29). Charge separation was induced by a 5 ns (FWHM) light pulse at 700 nm using a Nd:YAG pumped LDS 698 dye exciting ~70% of the reaction centers. Absorbance changes were followed from 5 ns to 20 μs using detecting flashes provided by an OPO Continuum (OPO Panther, type II) from 300 to 540 nm, frequency doubled for wavelengths less than 410 nm. For detection in the UV, a fluorescent glass (Sumita optical glass, Lumilas B) was used to convert the UV photons to the blue where the blocking filters perform better.

Measurements of the variable fluorescence yield in whole cells were used to quantify functional PS II relative to the WT using a Joliot-type flash detection spectrophotometer as previously described (30). Cells were suspended in 50 mM HEPES/KOH pH 7.5 at a concentration equivalent to an OD_{730} = 0.9 and were incubated for 10 minutes in the dark in 0.3 mM *p*-benzoquinone and 0.3 mM potassium ferricyanide prior to the start of the experiment. The cells were then incubated in the dark at room temperature in the presence of 20 μM DCMU and 20 mM NH_2OH, the latter added approximately 30 s before the start of the measurement. The variable fluorescence yield of PS II was then measured by detecting flashes following each of 20 saturating light flashes (18 Hz).

RESULTS

Gene Knock-out Mutations

The *crtP* (*pds*) and *crtQ* (*zds*) genes were deleted independently in *Synechocystis* sp. PCC 6803 as described in Materials and Methods. The *pds*$^-$ and *zds*$^-$ mutants were difficult to select for as the gene deletions caused the mutants to be acutely light sensitive. This photosensitivity is most probably due to the inability of the carotenoids with shorter conjugated chains to quench chlorophyll triplet states, which in the presence of light and oxygen lead to the formation of toxic singlet excited O_2 ($^1\Delta_g$) (31). Consequently, to drive genomic segregation to completion, the *pds*$^-$ and *zds*$^-$ mutants were selected on BG-11 containing 5 mM glucose plates prepared with fresh 200 μg/mL kanamycin and grown under very dim light (~0.1 μmol photons $m^{-2}s^{-1}$). The reduced light intensity resulted in a very low rate of cell growth. These knockout mutations also resulted in the complete loss of the PS II reaction centers in both mutant strains, as indicated by the absence of

fluorescence induction in the presence of DCMU and hydroxylamine (see Materials and Methods). Several failed attempts at the biochemical isolation of PS II complexes from thylakoid membranes (21) also indicated the absence of PS II. The absence of PS II is likely a consequence of the inability to assemble PS II complexes, where only phytoene or zeta-carotene is available as a replacement for β-carotene.

The PS I concentration of the mutants, on a per chlorophyll basis, was close to that of the WT strain, as equivalent loading of detergent solubilized thylakoid membranes (based on chlorophyll content) onto the DEAE column lead to similar recoveries of PS I complexes. However, the amount of chlorophyll isolated from the *pds*$^-$ and *zds*$^-$ strains (chlorophyll/cell) was approximately one-half that of the WT strain from cultures of the same volume (18 L) and optical density (OD_{730} ~ 1.5). In Figure 3a, the absorption spectrum of the WT PS I complex is compared to that of the *pds*$^-$ and *zds*$^-$ strains following normalization to the chlorophyll Q_y absorption band. Particularly noticeable in the absorption spectra of the mutants is the loss of absorption in the 450-525 nm region, indicating the loss of β-carotene biosynthesis in the mutants. Consistent with this spectrum and the loss of β-carotene and its derivatives, the PS I complexes isolated from the *pds*$^-$ and *zds*$^-$ strains are bluer in color than their WT homologues. In the *zds*$^-$ strain spectrum (Fig. 3a), however, there is an enhanced absorption in the 350-425 nm region which is attributed to the presence of the 7-conjugated double bond carotenoid zeta-carotene and its derivatives (Fig. 3b). Zeta-carotene absorbs maximally at ~400 nm in solvents with low polarizability (32). The *pds*$^-$ cores, on the other hand, show an absorbance spectrum that is essentially identical to that of pure Chl *a*, indicating the lack of synthesis of both β-carotene and zeta-carotene. HPLC analysis (see below) confirmed these observations. Instead of β-carotene or zeta-carotene, the *pds*$^-$ strain produces the 3-conjugated double bond carotenoid phytoene. Phytoene absorbs maximally at ~280 nm in solvents with low polarizability (32). In the red region, the maximum absorption corresponding to the Q_y transitions of the chlorophylls in the WT PS I complexes peaks at 680.6 nm. For the zeta-carotene desaturase and phytoene desaturase mutants, the maximum absorption of the Q_y transition was shifted to 678.8 and 679.0, respectively. Possible reasons for this will be discussed below. Fig. 3b shows the spectral subtractions of the Q_y normalized absorbance spectra, WT minus *pds*$^-$ and *zds*$^-$ minus *pds*$^-$. The former yields the absorbance spectrum of β-carotene, together with its isomers and hydroxy-derivatives, that are bound to the WT PS I complex while the latter, that of zeta-carotene and its isomers that are bound to the *zds*$^-$ PS I complex. The maximum height of the *zds*$^-$ carotenoid absorbance spectrum is approximately 35% of that of the WT carotenoid absorbance spectrum. As the extinction coefficients of beta- and zeta-carotene are practically equivalent, the loss of absorption indicates that some of the carotenoid binding sites in the PS I complexes of the *zds*$^-$ strain are devoid of carotenoids. This finding is also confirmed by the HPLC analysis below. Also noticeable in these spectral subtractions is the difference in shape of the cumulative absorbance of the carotenoids in the WT (mainly β-carotene) versus that in the *zds*$^-$ strain (all zeta-carotene). The absorbance peaks of zeta-carotene (385, 406, 432 nm) in the spectral subtractions are sharper and better defined while those of β-carotene (434, 468, 496 nm) are less so. This is mainly because linear carotenoids tend to have sharper absorption peaks than carotenoids with cyclic ends (32).

Pigment analysis

The PS I complex in the x-ray crystal structure is a trimer with each monomer binding 96 chlorophylls *a* (Chl *a*) and 22 carotenoid molecules. Figure 4a shows an HPLC chromatogram of the total pigment extract of WT PS I complex run on a reverse phase column. Three peaks for carotenoids are observed together with a peak for Chl *a*. The absorbance maxima of all of the carotenoid peaks are at 450 nm (not shown), suggesting that the different carotenoids found in PS I all have the same extent of carbon-carbon π-electron conjugation. Since the method used for elution was reverse-phase HPLC, we expect that the most non-polar molecules will elute last. We assign the peak eluting at ~30 min to β-carotene not only because of its position in

the elution profile but also because of its relative abundance compared to the other carotenoid peaks. This assignment was also confirmed by the observation of the same retention time and absorption spectrum for a β-carotene standard (not shown). Noticeable in this peak is a shoulder at ~32 min which we assign to several forms of *cis*-β-carotene. The absorbance spectrum of the sample eluting at that time shows a "*cis*-band", a feature present at ~140 nm to the blue of the red most absorption band of carotenoids. Owing to the C_{2h} symmetry present in all-*trans* carotenoids, this transition is absent or less prominent in all-*trans* carotenoids but becomes more visible in *cis* carotenoids because *trans*-to-*cis* isomerization breaks the C_{2h} symmetry (33,34). We assign the peak eluting at ~10 min to all-t*rans*-zeaxanthin and this is confirmed by an identical retention time and absorption spectrum of a standard zeaxanthin sample (not shown). Zeaxanthin (bottom of Fig. 1) is isoelectronic with β-carotene and contains two hydroxyl groups that are present in each of the terminal β-ionylidene rings, which makes it relatively more polar causing it to elute much earlier than β-carotene. The peak eluting at ~17 min is assigned to a mixture of *cis*-β-cryptoxanthin and/or isocryptoxanthin which were also found in substantial amounts in PS I preparations of *Synechococcus elongatus* (35). These two carotenoids only differ from each other by the position of the hydroxyl group on the ring (bottom of Fig. 1) and are expected to have identical absorption spectra (18,36). For simplicity, the mention of β-carotene$_{fam}$ (β-carotene family) will henceforth represent all the carotenoids (zeaxanthin, β-cryptoxanthin and isocryptoxanthin and their *cis*-*trans* isomers) "isoelectronic" (*i.e.*, the same number of π -conjugated double bonds) with β-carotene.

Figure 4b shows the HPLC chromatogram of the total pigment extract for the *zds*$^-$ PS I complex. The absorption spectra of all the carotenoid peaks have their absorption maxima at ~400 nm (not shown) which indicates that the carotenoids in this complex are isoelectronic. From the biosynthetic pathway of carotenoids for cyanobacteria shown in Fig 1, it is most likely that these carotenoids are isomeric zeta-carotenes which would accumulate in the absence of the *zds* gene. However, the possibility of a derivative form of zeta-carotene with cyclohexenyl or β–ionylidene rings cannot be completely discounted as lycopene cyclase is still present in this mutant and could use zeta-carotene as a substrate. These derivatives of zeta-carotene would also show absorption spectra similar to acyclic or linear zeta-carotene as the extent of their π-electron conjugation is not affected by the cyclization of the ends of the molecule. For simplicity, the mention of zeta-carotene$_{fam}$ (zeta-carotene family) in this paper represents all the "isoelectronic" carotenoids with 7 π-conjugated double bonds produced in this mutant. The main peak eluting at ~29 min is all-*trans* zeta-carotene while the small shoulder before that eluting at ~27 min is a *cis* zeta-carotene. A minor peak eluting at ~33 min is assigned to another form of zeta-carotene, perhaps another *cis*, where the *cis* configuration is at or near the end of the π electron conjugation. The "*cis* band" in this form has a lower intensity than in central-*cis* carotenoids (34).

For the *pds*$^-$ mutant complex (Fig. 4c), only one distinct pigment peak is present in addition to Chl *a*. The peak eluting at ~30 min is assigned to phytoene (maximum absorbance at 288 nm) (not shown). The earlier peak at ~5 min is due to the solvent front acetone/methanol in which the pigment extracts were dissolved before injection into the HPLC.

Table 1 summarizes the approximate stoichiometry of the chlorophyll and carotenoids extracted from the WT and mutant PS I complexes. The number of carotenoids present here per WT complex (~26, normalized to 96 chlorophylls) is slightly greater than the 22 reported in the *Thermosynechococcus elongatus* crystal structure (*2*), possibly reflecting differences in the preparations. Noticeable in Table 1 is the reduced amount of carotenoid in the mutant PS I complexes. Because the native protein evolved binding β-carotene$_{fam}$, zeta-carotene$_{fam}$ and phytoene are not likely to produce a tight fit in the carotenoid binding sites as the more saturated carotenoids are non-planar at the ends owing to more sp^3-hybridized carbon centers with tetrahedral geometry and greater rotational degrees of freedom. The carotenoids are therefore more loosely bound and may either not have bound *in vivo* or may have been lost during the purification process.

X and Q-band EPR

According to the x-ray crystallographic structure of the PS I reaction center of *Thermosynechococcus elongatus* (2), several carotenoids are located in the immediate vicinity of each of the phylloquinones of PS I. To check if a change in the number and structure of carotenoids in PS I has had an effect on the EPR spectra of the electron acceptors, X-band and Q-band EPR spectra were recorded. X-band (9.4 GHz) EPR spectroscopy was performed on the WT and mutant (*pds*$^-$ and *zds*$^-$) PS I complexes to examine iron-sulfur clusters F_A^-/F_B^-. The pH of the samples was adjusted to 10.0 and sodium dithionite was added to a final concentration of 50 mM (see Materials and Methods) and the EPR spectrum was recorded at 15 K. The g-values and the relative spin concentrations of reduced F_A (g = 2.05, 1.94, 1.85) and F_B (g = 2.07, 1.92, 1.88) in the *pds*$^-$ and *zds*$^-$ PS I mutants were identical to those of the WT (Fig. 5). Similar spectra were recorded when the samples were adjusted to pH 8.3 in the presence of sodium ascorbate and illuminated during freezing to 15 K (data not shown). Thus, the absence of and/or replacement of β-carotene$_{fam}$ with carotenoids of shorter conjugated length in PS I does not affect either the ability to form F_A^-/F_B^- or the electronic structures of the F_A^-/F_B^- iron sulfur clusters at low temperature.

Figure 6 shows the Q-band (34 GHz) EPR spectra of the WT and the mutant PS I complexes after photoaccumulation at 205 K, a technique that generates A_1^- and F_X^- in a background of chemically prereduced F_A^-/F_B^-. Note that at 205K, signals from the iron-sulfur clusters are not detectable, hence the spectra shown are mainly due to A_1^- and perhaps a small amount of A_0^-. The WT and mutant spectra very closely resemble each other. At 34 GHz, the field-dependent g-anisotropy dominates the spectrum of A_1^- which allows for the partial resolution of the turning points at g_{xx} = 2.0062 and g_{zz} = 2.0021, values that agree with previous studies (26,37-39). Since the g_{yy} component of the tensor is hidden by the methyl proton hyperfine lines that arise from the high spin density at carbon 2 of the phylloquinone anion radical (A_1^-) it is hard to determine its exact value. To better resolve the value of the g_{yy} tensor, PS I from *Synechocystis* sp. PCC 6803 cells grown in 92% D_2O were used in a similar experiment (37) to suppress the intensity of the proton hyperfine couplings. Deuteration resulted in the narrowing of the line widths of the g-components and revealed a value of 2.0051 for the g_{yy} component in WT PS I (37). The Q-band EPR spectra indicate that the *g*-tensor values and the hyperfine couplings for phyllosemiquinone are virtually identical in the WT and mutant strains. We conclude that the ability to photoreduce phyllosemiquinone and the electronic structure of phyllosemiquinone in the WT and mutant PS I reaction centers are insensitive to the absence and/or the replacement of β-carotene$_{fam}$ with zeta-carotene$_{fam}$ or phytoene.

Electron transfer from A_1^- to F_X

Figure 7 shows kinetic traces of the absorbance changes at 380 and 480 nm after the flash-induced formation of the phyllosemiquinone anion A_1^- for the WT, *pds*$^-$ and *zds*$^-$ PS I complexes. The transients were best fit with double exponential functions. Similar kinetic profiles were also determined at different wavelengths from 300-540 nm in whole cells and PS I complexes and the kinetic data were subjected to global fit analysis. The results are summarized in Table 2. For the WT PS I complexes, the faster decay component has a $t_{1/2}$ = 8-9 ns (20-25% of total decay amplitude estimated by comparing the relative amplitudes of the UV signals at 380-390 nm of Fig. 8, see below) while the slower component has a $t_{1/2}$ = 152-180 ns (~75-80% of total decay). These time constants and relative amplitudes are similar to previous determinations on different cyanobacterial PS I preparations (9) although considerable variability in the relative amplitudes of the fast and slow phases have been found with PS I complexes from the eukaryote, spinach, *C. reinhardtii* and *Chlorella*. In spinach, depending on preparation methods, the ratio of the amplitudes of the fast to the slow component varied considerably from 2:1 to 1:2 while in whole cells of *C. reinhardtii* and *Chlorella*, the difference spectra showed a 1:2 and 1:1 relative amplitudes, respectively. For the *pds*$^-$ and *zds*$^-$ strains, the relative amplitudes of the fast and slow phases are similar to the WT. However, the time constants in the PS I mutant complexes are somewhat longer, particularly for the slow phase (1.5 times) compared to WT (see Table 2).

To verify that the fast and slow phases indeed arise from A_1^- oxidation, the global exponential fits for these phases were compared in the UV and near-UV where the phyllosemiquinone minus phylloquinone difference spectrum is expected to contribute most strongly. Fig. 8 shows the A_1^-(FeS) - A_1(FeS)$^-$ difference spectra from 300-540 nm obtained by global exponential fit analysis of the kinetic data for the WT, *pds*$^-$ and *zds*$^-$ PS I complexes. The slow phase UV and near-UV difference spectrum of the WT show peaks at 375 nm, 405 and 430 nm, with a shoulder at 340 nm and a minimum at 315 nm. In the fast phase difference spectrum, there is a peak at 400 and 425 nm, but the shorter wavelength peak, the shoulder and the minimum are all shifted by 10-15 nm to the red with respect to the slow phase. In the case of the mutants, however, the fast and slow-phase difference spectra look more similar to each other except for the presence of a 340 nm shoulder in the slow-phase difference spectra and a small 385 nm feature present in the fast-phase difference spectra. The contribution of FeS - FeS$^-$ to A_1^-(FeS) - A_1(FeS)$^-$ is expected to be relatively small in this region. With the possible exception of a contribution from $FeS_{[X]}$ - $FeS_{[A/B]}^-$ to the spectrum of the slow phase (e.g. at 340 nm), the similarity of the fast and slow-phase difference spectra to each other and to the *Chromatium* menasemiquinone-menaquinone (Vit K_2^- - Vit K_2) difference spectra (40) support the attribution of the fast and slow phases largely to the oxidation of phyllosemiquinone. The PS I pyllosemiquinone-phylloquinone (Vit K_1^- - Vit K_1) difference spectra, however, appear to be shifted to shorter wavelength by about 30 nm compared to the difference spectra reported by Romijn and Amesz (40).

The same figure (Fig. 8) shows the absorption difference spectra of the fast and slow-phases of the A_1^-(FeS) - A_1(FeS)$^-$ difference spectra of the WT, *zds*$^-$ and *pds*$^-$ PS I cores to 540 nm. Some of the most marked features of the visible difference spectrum are located at $\geq$ 440 nm where the contribution of the phyllosemiquinone minus phylloquinone difference spectrum is expected to be small and relatively flat (40). The A_1^-(FeS) - A_1(FeS)$^-$ for the WT shows a marked second derivative-shaped signal centered at ~450 nm for both the fast and slow phases. Another derivative-shaped signal is centered at ~506 nm for the fast phase and ~500 nm for the slow phase. The spectral differences between the fast and slow phases in this region have not been previously reported, as the earlier work did not extend beyond 500 nm (*42*). All of these features have been attributed to electrochromic band shifts of carotenoids coupled to A_1^- reduction (11,12). The construction of the *pds*$^-$ and *zds*$^-$ strains provides a test of these assignments. As shown in Fig. 8, the loss of β-carotene$_{fam}$ results in the complete disappearance of the 500 and 506 nm features but only a small change in the 450 nm-centered feature. Clearly the former is due entirely to β-carotene$_{fam}$ while the latter is not. The absence of the 500 and 506 nm features in the *pds*$^-$ and *zds*$^-$ spectra is caused either by the replacement of β-carotene$_{fam}$ by more saturated carotenoids, phytoene or zeta-carotene, respectively, which are at least 50 nm blue-shifted compared to β-carotene$_{fam}$, or the absence of carotenoid in the carotenoid-binding sites that are nearest to A_1. The second derivative-shaped feature centered at 450 nm is likely due to an electrochromic band shift of a chlorophyll or chlorophylls located close to A_1^-. The minimum of this signal appears at 448 and 452 nm for the fast and slow phases, respectively.

Also part of the fit for the global decomposition of the transient kinetics is a component that remains following the relaxations in the submicrosecond range. As the only species remaining are $P700^+$ and $FeS_{[A/B]}^-$, this component corresponds to the difference spectrum $P700^+FeS_{[A/B]}^-$ - $P700FeS_{[A/B]}$. Because the contribution of the $FeS_{[A/B]}^-$ - $FeS_{[A/B]}$ is so much smaller than that of $P700^+$ - P700, this spectrum corresponds primarily to the latter. This difference spectrum, shown in Fig. 9, shows a large bleaching at 435 nm and a derivative-shaped spectrum centered at about 518 nm. The latter feature disappears in the $P700^+FeS_{[A/B]}^-$ - $P700FeS_{[A/B]}$ difference spectrum in the *pds*$^-$ and *zds*$^-$ strains, indicating that this feature is most likely due to a β-carotene$_{fam}$ that is located close to P700.

To better resolve the spectra arising from carotenoid electrochromism coupled to A_1^-(FeS) - A_1(FeS)$^-$ and to $P700^+$ $FeS_{[A/B]}^-$ - P700 $FeS_{[A/B]}$, we calculated the double difference spectra, [A_1^-(FeS)

- $A_1(FeS)^-]_{WT}$ – $[A_1^-(FeS)$ - $A_1(FeS)^-]_{mutant}$ and $[P700^+FeS_{[A/B]}^-$ - $P700FeS_{[A/B]}]_{WT}$ - $[P700^+FeS_{[A/B]}^-$ - $P700FeS_{[A/B]}]_{mutant}$ for the fast and slow-phases of $A_1^-(FeS)$ - $A_1(FeS)^-$ and for $P700^+FeS_{[A/B]}^-$ - $P700FeS_{[A/B]}$ (Fig. 10). The spectra were normalized to the 430 nm signal of $P700^+FeS_{[A/B]}^-$ - $P700FeS_{[A/B]}$ nm measured at 20 μs. In principle, all absorbance changes other than those arising from the carotenoids alone should disappear. It should be kept in mind, however, that spectral subtractions in the region of strong chlorophyll absorption correspond to differences between two large signals, thus creating a greater uncertainty in the difference spectra in this region. The A_1 double difference for the WT - *zds*$^-$ and for the WT - *pds*$^-$ both show very similar three peaked differences, consistent with their arising from electrochromic red-shifts of carotenoids. Both the positions of the inflections (corresponding to the carotenoid absorbance maxima) and their displacement from each other (30-35 nm) are consistent with their identification with the β-carotene$_{fam}$. A comparison of the fast and slow phases in both cases indicates that the slow phase is displaced to the blue relative to the fast phase by approximately 6 nm. The difference between the two phases implies that the carotenoids that detect the fast and slow phases are located in different environments. This difference in the locations of the carotenoid band shifts is also observed in WT cells (Fig. 11), indicating that it is an intrinsic property of the reaction center and not an artifact of detergent isolation. The reasons for this displacement will be discussed below.

Fig. 10 also shows the P700 double difference spectrum for the WT and each of the mutants. While there are some differences in the 400-450 nm range, these double difference spectra also indicate the clear involvement of β-carotene$_{fam}$ in electrochromism tied to P700 oxidation. By taking the P700 double difference of *zds*$^-$ minus *pds*$^-$, band shifts are apparent that likely arise from the two longer wavelength peaks of zeta-carotene$_{fam}$. These are responsible for the differences observed in the WT minus *zds*$^-$ and the WT minus *pds*$^-$ difference spectrum between 400 and 450 nm. Thus, the carotenoid or carotenoids that sense the oxidation of P700 are β-carotene$_{fam}$ in the WT and are replaced by zeta-carotene$_{fam}$ in the *zds*$^-$ strain. The double difference *zds*$^-$ minus *pds*$^-$ in the A_1 case leaves smaller residuals than those observed for P700, possibly indicating a lower probability of the zeta-carotene$_{fam}$ replacing β-carotene$_{fam}$ in the neighborhood of the phylloquinones.

Charge recombination from F_A/F_B^- to $P700^+$

The slowing of the slow phase of oxidation of A_1^- in the mutants compared to WT could reflect a change in the reduction potential of A_1/A_1^- (Eq. 1). Any mutation-induced changes in the reduction potential of A_1/A_1^- can be quantified by measuring the rate of charge recombination ($V_{obs,}$ Eq. 2) between $P700^+$ and F_A/F_B^-, assuming that the rate of acceptor side equilibration is rapid relative to the rate of charge recombination and that the intrinsic rate of charge recombination (k_{in} = 95 us (41)) of $P700^+A_1^- \rightarrow P700A_1$ does not change in the mutants. The rate of charge recombination should then be proportional to the equilibrated concentration of A_1^- (eq. 1) determined by equilibrium constant K_{AF} (Eq. 3). An increase in the reduction potential of A_1/A_1^- would consequently accelerate charge recombination. The rate of charge recombination between $P700^+$ and F_A/F_B^- was measured by saturating flash excitation followed by detection at 435 nm, a minimum of the $P700^+$- P700 difference spectrum (Fig. 9). Figure 12 shows an increase in the rate of charge recombination from a $t_{1/2}$ of 35 ms (τ = 51 ms) in the WT to a $t_{1/2}$ of 19 ms (τ = 27 ms) in the *zds*$^-$ strain (Fig. 12). A similar experiment performed on PS I complexes of WT and the *pds*$^-$ strain gave a $t_{1/2}$ of 33 and 24 ms, respectively (not shown). The change in recombination rate corresponds to an increase in reduction potential of A_1/A_1^- of 16 mV and 8 mV, respectively, for the *zds*$^-$ and *pds*$^-$ complexes.

Eq. 1 $\Delta E' = 59\log(K_{AFwt}/K_{AFmut})$

where

$K_{AFwt}/K_{AFmut} = [(k_{in}/V_{obswt})-1]/[(k_{in}/V_{obsmut})-1]$

Eq. 2 $V_{obs} = k_{in}[1/(K_{AF}+1)]$

Eq. 3 $A_1^-(F_A/F_B) \overset{K_{AF}}{\rightleftarrows} A_1(F_A/F_B)^-$

DISCUSSION

β-carotene$_{fam}$ is needed for PS II assembly

Carotenoids play multiple roles in photosynthesis. They are accessory pigments used for light-harvesting and for photoprotection in chlorophyll-protein complexes by quenching of chlorophyll triplet states (42). We show here that the replacement of β-carotene$_{fam}$ with shorter conjugated chain carotenoids in *Synechocystis* sp. PCC 6803 results in the loss of PS II complexes in the thylakoid membranes. This observation is consistent with the observations of Trebst and Depka (43) in which inhibition of phytoene desaturase by norflurazon and fluridone results in the loss of the D1 polypeptide. Either the inability to quench chlorophyll triplet states accelerates the rate of D1 photodamage and degradation or the lack of an appropriately shaped carotenoid results in an inability to correctly assemble PS II reaction centers. In either case, accumulation of PS II in the thylakoid membranes is prevented.

Spectroscopic characterization

The replacement or absence of β-carotene and its hydroxylated derivatives results in a 2 nm blue shift of the Q_y absorption maximum of the Chls in in the PS I complexes From the 2.5 Å X-ray crystallographic structure of PS I in *Thermosynechococcus elongatus*, close associations are observed between the carotenoids and the chlorophylls of the reaction center (2,3). Because the ringed carotenoids (β-carotene, zeaxanthin, β-cryptoxanthin and isocryptoxanthin) are replaced by ones with shorter conjugation (zeta-carotene or phytoene) or no carotenoid at all, structural adjustments are to be expected. Such structural changes could result in alterations in local dielectric, in excitonic interaction between pigments, or in a loss of carotenoid-associated chlorophyll binding sites. That the last two of these contribute to the above mentioned absorbance changes will be documented in a forth-coming publication.

Forward electron transfer from A_1^- to F_X

Brettel, Setif and Mathis (44) showed in $P700^+A_1^-$ charge recombination experiments with prereduced F_A and F_B at 10K ($t_{1/2}$ ≈150 μs) that the A_1^- - A_1 difference spectrum bears a close resemblance to the absorbance difference spectrum for Vit K_1^-• - Vit K_1 (40). This resemblance is consistent with the presence of phylloquinone in PS I complexes (45) and provided strong evidence for the identification of A_1^- with phyllosemiquinone. Brettel and coworkers (44) were the first to measure the UV and visible region absorbance changes associated with the forward oxidation of A_1^-. The A_1^-(FeS) - A_1(FeS)$^-$ absorbance difference spectra were measured in PS I complexes from the cyanobacteria *Synechocystis* sp. PCC 6803 (8) and *Synechococcus* sp. (11) and from spinach (46). These spectra have now been examined with improved signal/noise and over a more extended wavelength range in PS I complexes from *Synechocystis* sp. PCC 6803 (the present work) and in whole cells of *C. reinhardtii* (47). These spectra bear a close resemblance in the UV to the difference spectra generated by $P700^+A_1^-$ charge recombination (44).

The forward oxidation of A_1^- has been shown to be biphasic with half times (relative amplitudes) of 25 (65%) and 150 (35%) ns in spinach PS I complexes (46) and 7 (33%) and 190 (66%) ns in *Synechocystis* sp. PCC 6803 (8). Similar biphasic kinetics have been observed in *Chlorella sorokiniana* (12) and in *C. reinhardtii* (14). The A_1^-(FeS) - A_1(FeS)$^-$ difference spectra for the two phases are shown in Fig. 8 for WT *Synechocystis* sp. PCC 6803 and the two knockout strains *pds*$^-$ and *zds*$^-$. They both bear an overall resemblance in the UV to *Chromatium* Vit K_2^-• - Vit K_2 and to the *in vitro* Vit K_1^-• - Vit K_1 difference spectrum (11,40). The spectra observed here peak at 375-380 nm instead of the 390 nm observed in the *in vitro* spectrum and are shifted by about 30 nm to shorter wavelength compared to the *Chromatium* difference spectrum. There is also additional fine structure in the biological spectra, as observed by Brettel (8,11). In the case of the WT, the slow and fast phases of A_1^- oxidation show similar spectral components, the relative amplitudes of which are different. A component at 385 nm appears to dominate in the fast phase spectrum while one at 378 nm dominates in that of the slow phase. Also a shoulder at 340 nm in the slow phase appears to be missing in the fast phase. The fast and slow phase UV spectra are more similar in the case of the *pds*$^-$ and *zds*$^-$ strains. In the two mutants, the 385 nm component is smaller

than the 378 and 405 nm components resulting in a closer resemblance in the spectra of the two phases. These observations argue in favor of the fast and slow phases arising from the same chemical species, possibly in somewhat different environments, the differences for which are more marked in the WT difference spectrum. It is also possible that there is an additional small contribution from F_X to F_A/F_B electron transfer that contributes to the slow phase in all three strains. The shoulder at 340 nm in the slow phase might arise from such a contribution.

The Vit K_1^-• - Vit K_1 *in vitro* difference spectrum shows only small and flat absorbance changes above 440 nm (40). In this range there are marked features (450-470 nm and 500-520 nm) in the A_1^-(FeS)-A_1(FeS)$^-$ difference spectra of the fast and slow phases that most likely come from electrochromic band shifts of pigments located in close proximity to A_1, reflecting the anionic charge present in the A_1^- state. The pigments responsible for these electrochomic band shifts were suggested to be carotenoids (11,12). A comparison of the A_1^-(FeS) - A_1(FeS)$^-$ from the WT and from the two carotenoid mutants indicates slight modifications in the 450-470 nm range and large differences in the 500-520 nm range. In both the *pds*$^-$ and the *zds*$^-$ strains the band shifts in the 500-520 nm range have completely disappeared in the difference spectra of both phases. However the large second derivative shaped signal in the 430-470 nm range has remained largely intact, including the displacement of the fast phase minimum at 448 nm to 452 nm in the slow phase. A derivative-shaped shoulder present at 460 nm in the WT fast phase has disappeared in the mutants. By taking the double difference $[A_1^-(FeS) - A_1(FeS)^-]_{WT} - [A_1^-(FeS) - A_1(FeS)^-]_{mutant}$, one obtains the spectra shown in Fig. 10. Here one can see that there are three electrochromic bands that undergo a red shift in both the fast and slow phases. The 30-35 nm spacing between these shifts is consistent with their arising from β-carotene$_{fam}$. It is clear that the band shifts are not located in the same positions for the fast and slow phases, with the band shifts displaced by approximately 6 nm to higher wavelength for the fast phase as compared to the slow phase. This observation supports the idea that the A_1 species in each of the two phases is present in a different environment, giving rise to electrochromic band shifts of a different set of carotenoid pigments. That the second derivative shaped feature in the 430-470 nm range remains prominent in the mutant difference spectra, despite the absence of carotenoids absorbing in this range, argues that the remaining band shift most likely arises from one or more chlorophyll molecules.

There has been considerable controversy concerning whether one or both of the phylloquinones are active for electron transfer in PS I to explain the biphasic kinetics in the electron transfer step between A_1^- and the FeS clusters. Setif and Brettel (8,46) had initially attributed the presence of the biphasic kinetics of A_1^- oxidation to the equilibrium between A_1 and F_X, the reduction potentials of which were proposed to be close. The fast phase would then arise from the establishment of the equilibrium $A_1^-F_X \rightleftarrows A_1F_X^-$ while the slow phase would be limited by the electron transfer from F_X to the F_A/F_B centers (8,46). Joliot and Joliot (12), have argued that, as the electron transfer from A_1^- to F_X is electrogenic (13), then if the fast phase were indeed the establishment of the equilibrium concentrations of A_1^- and F_X^-, its relative amplitude should be sensitive to the transmembrane electric field. They showed that, on the contrary, the relative amplitudes of the fast and slow phases were independent of the membrane potential. Leibl and coworkers (13,48) have also concluded from photovoltage measurements that the rate of electron transfer from F_X^- to F_A/F_B ($\tau \leq 50$ ns) is faster than that of the slow phase of A_1^- oxidation. Both of these experimental observations thus argue against the equilibrium model and in favor of one where either the two quinones operate independently in a two pathway model or where only one of the quinones is functional, but where there is a heterogeneity in the centers giving rise to two different rate constants for A_1^- to F_X electron transfer (12).

Site-directed mutations have been constructed in *C. reinhardtii* and in *Synechocystis* sp. PCC 6803 in the region of each of the two phylloquinones. Mutations PsaA-W693F and PsaB-W673F (10,14) resulted in a substantial slowing, respectively, of the slow and fast phases of A_1^- forward oxidation. In each case, the rates of the complementary fast and slow phases, respectively, were unchanged as were the relative amplitudes of the fast and slow phases. Similar

results were obtained with the PsaA- and PsaB-side mutations, PsaA-S692C and PsaB-S672C in *Synechocystis* sp. PCC 6803, although the effect on the fast kinetic phase of the PsaB-side mutant was not as pronounced as in the PsaB-W673F (10,47). These results argue in favor of the two-pathway model in which the fast phase would arise from the PsaB-side and the slow phase the PsaA-side. Also supporting the two-pathway model are EPR-detected kinetics of $P700^+A_1^-$ charge recombination at 100K following illumination at 205K in the presence of sodium dithionite. Two phases are observed for charge recombination the slower of which is lost upon illumination in the PsaA-W693H and L mutants (49). Xu and coworkers (10), while confirming the room temperature optical results with both sets of mutants, were unable to observe a slowing of the fast phase using transient EPR. They concluded that the PsaA-branch is active but that there was no EPR-based evidence for electron transfer up the PsaB-branch. Thus, according to their data, a unidirectional scheme using the A-pathway of electron transfer with center heterogeneity could not be ruled out. The inability of Xu et al. (10) to observe the same relative amplitude of fast phase by transient EPR as they observe in optical experiments, however, may be due to the inability of transient EPR to detect, even indirectly, a kinetic phase of <10 ns, especially when the fast kinetic phase represents a minority of the electron flux to F_X.

The present work adds support for the two-pathway model and provides additional spectroscopic markers with which to distinguish the two electron transfer pathways. We have shown here that the carotenoid pigments that act as electrochromic detectors for the fast and slow phases are different and are shifted 6 nm with respect to each other. That these same difference spectra are observed in PS I complexes and in PS I in whole cells, with similar rates for the fast and slow phases and with similar relative amplitudes would argue against the two phases originating from center heterogeneity. That in the β-carotene deficient *pds*$^-$ and *zds*$^-$ strains, the A_1^-(FeS) - A_1(FeS)$^-$ difference spectra of the fast and slow phases become practically identical with little change in relative amplitude compared to WT also argues that the spectral differences between the fast and slow phases and the biphasic electron transfer do not arise from a heterogeneity between PS I reaction centers. The spectral differences in the two phases most likely arise then from carotenoids with different conformations and/or configurations or carotenoids in different environments associated with each of the two phylloquinones. These spectral differences associated with each phase thus argue for the participation in electron transfer of both the PsaA-side and PsaB-side quinones.

Examination of the *Thermosynechococcus elongatus* PS I X-ray crystal structure (2) indeed shows that there are structural differences in the carotenoids associated with the PsaA- and PsaB-sides of the reaction center in the immediate vicinity of the phylloquinones. Two β-carotene$_{fam}$ carotenoids with *cis* double bonds are found near the phylloquinone on the PsaA-side while only one is found on the PsaB-side. On the PsaA-side, there is a 9,13-di-*cis* (see numbering in Fig. 1) located at a distance of 19 Å from PhQ_A. (edge-to-edge distance) There is also a 13-*cis* β-carotene$_{fam}$ carotenoid 25 Å away. On the PsaB-side, the only *cis*-β-carotene$_{fam}$ carotenoid found near PhQ_B is 9-*cis*, located 22 Å away. Hashimoto and Koyama (50) have shown in *n*-hexane that the absorption spectrum of 9-*cis* β-carotene is 6 nm shifted to the blue compared to the corresponding all-*trans* isomer. The 13-*cis* isomer, on the other hand, is shifted by 11 nm to the blue, again, compared to the corresponding all-*trans* isomer. In general, the nearer the *cis* double bond is to the center of the carotenoid, the greater the extent of the blue shift (50). A 9,13-di-*cis* β-carotene is expected to be even more blue shifted than its corresponding mono-*cis* isomers. It is most likely that the carotenoids nearest to the phylloquinones all experience electrochromic effects but that the cumulative effect of having two *cis*-carotenoids (having a total of three *cis* double bonds) on the PsaA-side shifts the overall absorption spectrum of the carotenoids on the PsaA-side 6 nm to the blue compared to the carotenoids on the PsaB-side with only one *cis* double bond between them.

The differences in the minima of the second derivative shaped feature in the 430-470 nm range between the fast and slow phases also likely reflect a difference in the electrochromic effects of the PsaA- and PsaB-side phyllosemiquinone anions on nearby chlorophylls. Consistent with this observation, Dobek and

Brettel (51) have recently reported differences in the spectra of the fast and slow phases of A_1^- oxidation in the 660-694 nm range that likely reflect electrochromic effects on different reaction center chlorophylls. The absorbance spectra of most of the PS I component chlorophylls are however not known, making it difficult to make structural assignments to the detecting chlorophylls.

The *zds*$^-$ and *pds*$^-$ strains both show a marked slowing of the slow phase of A_1^- oxidation ($t_{1/2}$ ~ 250 ± 18 ns) compared to WT ($t_{1/2}$ ~ 170 ±15 ns). There may also be a slight slowing of the fast phase, but the alteration in rate, if it exists, is within the noise level of the measurement. The mutant strains also show an acceleration of the rate of charge recombination relative to WT. These observations are understandable in terms of a model proposed by Agalarov and Brettel (9) in which $A_1^- \rightarrow F_X$ electron transfer is exergonic on one side of the reaction center and endergonic on the other, most likely the PsaB- and PsaA-sides, respectively. We propose that the replacement of β-carotene$_{fam}$ by shorter chain carotenoids or the loss of β-carotene$_{fam}$ in the mutant strains results in the raising of the reduction potential of the phylloquinones. As the Marcus curve is parabolic for the $A_1^- \rightarrow F_X$ electron transfer, a given change in the free energy of the reaction will have a larger effect on the reaction rate of the endergonic than on the exergonic reaction (Fig. 13). This is indeed what we observe (Table 2, Fig. 7).

The rate of charge recombination is governed by the product of the intrinsic rate (k_{in}) of charge recombination between $P700^+$ and A_1^- times the concentration of A_1^-. The latter is determined by the relative reduction potentials of the A_1/A_1^- and $(F_A/F_B)/(F_A/F_B)^-$ redox couples. The more positive the reduction potential of A_1/A_1^- the higher the concentration of A_1^- following charge separation and the higher the rate of charge recombination. Assuming the intrinsic rate of $P700^+A_1^-$ recombination to be the same in the mutants and WT, then the higher rate of charge recombination in the mutants reflects an increase in the reduction potential of A_1/A_1^-. Recombination should occur predominantly through the PsaA-side phylloquinone, the more positive of the two resident quinones. The more rapid recombination in the mutants is thus consistent with the slowed rate of the slow-phase forward reaction, with both arising from an increased reduction potential of the PsaA-side phylloquinone (Fig. 13). The 1.4 to 1.8-fold increase in rate of charge recombination corresponds to an increase in reduction potential of A_1/A_1^- of 8-16 mV. While less visible, it is likely that the PsaB-side phylloquinone has also undergone a similar increase in reduction potential. The existence of endergonic and exergonic components of the kinetics of oxidation of A_1^- is most consistent with the bidirectional model.

Fig. 2 shows the cluster of carotenoids located close to each of the phylloquinones in the X-ray crystal structure of PS I. The increase in reduction potential of the phylloquinones in the mutants suggests that the loss/replacement of the carotenoids close to the phylloquinone in the WT results in a stabilization of the phyllosemiquinone relative to phylloquinone. One of the striking characteristics of the phylloquinones of PS I is their very low reduction potential. These have been estimated to be -531 mV and -686 mV for the PsaA- and PsaB-side PhQ/PhQ^- redox couples, respectively (52). The carotenoids are apparently one contributing factor to this low potential, a role for these molecules in photosynthesis not previously appreciated.

The small increase in the A_1/A_1^- reduction potential associated with the loss/replacement of the carotenoid could result from a small conformational shift of the peptide backbone in the vicinity of the phylloquinone, a factor that Ishikita and Knapp (52) have signaled as being a determining factor for quinone redox behavior in PS I. We have also found that the loss/replacement of carotenoid results in the depletion of the PsaF and PsaL subunits in the isolated complex along with some long–wavelength chlorophylls (manuscript in preparation). Van der Est and coworkers (53) have argued that the loss of PsaF in a *psa*F deletion mutant (accompanied by the loss of chlorophylls 1138 and 1139) could influence the redox properties of PhQ_A by increasing access to bulk water. These authors report, relative to WT PS I complexes, an increased rate of PhQ_A^- oxidation by F_x in the presence of Triton X-100 but a slowing of the rate by 10% in the presence of β-DM, the detergent used here. The slowing of the slow

phase of the A_1^- oxidation kinetics that we observe here in the *pds*$^-$ and *zds*$^-$ mutants is larger (50%) relative to WT (Table 2, Fig. 7) than what was reported by van der Est and coworkers in *Synechococcus* sp. PCC 7002 (53) and observed here both *in vivo* and in isolated PS I complexes from *Synechocystis* sp. PCC 6803. While the relative amplitudes of the effect on rate may be due to species differences, it is likely that the loss/replacement of carotenoid, with consequences for both PsaF and chlorophyll binding, enhances the impact on the reduction potential of PhQ_A/PhQ_A^-, beyond what is observed by deletion of PsaF alone. Although we interpreted above the difference in kinetic effects of carotenoid loss/replacement on the relative energetics of the PsaA- and PsaB- branches, it is also possible that the structural perturbations associated with the carotenoid loss/replacement have a larger impact on A_1/A_1^- reduction potential on the PsaA-side.

REFERENCES

1. Kobayashi, M., Watanabe, T., Nakazato, M., Ikegami, I., Hiyama, T., Matsunaga, T., and Murata, N. (1988) *Biochim. Biophys. Acta* **936**, 81-89
2. Jordan, P., Fromme, P., Witt, H. T., Klukas, O., Seanger, W., and Krauss, N. (2001) *Nature* **411**, 909-917
3. Fromme, P., Jordan, P., and Krauss, N. (2001) *Biochim. Biophys. Acta* **1507**, 5-31.
4. Setif, P., Fischer, N., Lagoutte, B., Bottin, H., and Rochaix, J.-D. (2002) *Biochim. Biophys. Acta* **1555**, 204-209
5. Wynn, R. M., and Malkin, R. (1988) *Biochemistry* **27**, 5863-5869
6. Farah, J., Rappaport, F., Choquet, Y., Joliot, P., and Rochaix, J.-D. (1995) *EMBO J.* **14**, 4976-4984
7. Hippler, M., Reichert, J., Sutter, M., Zak, E., Altschmied, L., Schroeer, U., Herrmann, R. G., and Haehnel, W. (1996) *EMBO J.* **15**, 6374-6384
8. Brettel, K. (1998) in *Photosynthesis: Mechanism and Effects (Garab, G., ed.)* Vol. I, pp. 611-614, Kluwer Academic Publishers, Dordrecht, The Netherlands
9. Agalarov, R., and Brettel, K. (2003) *Biochim. Biophys. Acta* **1604**, 7-12
10. Xu, W., Chitnis, P. R., Valieva, A., van der Est, A., Brettel, K., Guergova-Kuras, M., Pushkar, Y. N., Zech, S. G., Stehlik, D., Shen, G., Zybailov, B., and Golbeck, J. H. (2003) *J. Biol.Chem.* **278**, 27876-27887
11. Brettel, K. (1988) *FEBS Lett.* **239**, 93-98
12. Joliot, P., and Joliot, A. (1999) *Biochemistry* **38**, 11130-11136
13. Leibl, W., Toupance, B., and Breton, J. (1995) *Biochemistry* **34**, 10237-10244.
14. Guergova-Kuras, M., Boudreaux, B., Joliot, A., Joliot, P., and Redding, K. (2001) *Proc. Natl. Acad. Sci. USA* **98**, 4437-4442
15. Cohen, R. O., Shen, G., Golbeck, J. H., Xu, W., Chitnis, P. R., Valieva, A. I., Van der Est, A., Pushkar, Y., and Stehlik, D. (2004) *Biochemistry* **43**, 4741-4754
16. Fairclough, W. V., Forsyth, A., Evans, M. C. W., Rigby, S. E. J., Purton, S., and Heathcote, P. (2003) *Biochim. Biophys. Acta* **1606**, 43-55
17. Ramesh, V. M., Gibasiewicz, K., Lin, S., Bingham, S. E., and Webber, A. N. (2004) *Biochemistry* **43**, 1369-1375
18. Britton, G. (1995) in *Carotenoids* Vol. 1B, pp. 13-62, Birkhaeuser, Basel
19. Nixon, P. J., Trost, J. T., and Diner, B. A. (1992) *Biochemistry* **31**, 10859-10871
20. Rogner, M., Nixon, P. J., and Diner, B. A. (1990) *J. Biol. Chem.* **265**, 6189-6196
21. Tang, X.-S., and Diner, B. A. (1994) *Biochemistry* **33**, 4594-4603
22. Rippka, R., Deruelles, J., Waterbury, J. B., Herdman, M., and Stanier, R. Y. (1979) *J. Gen. Microbiol.* **111**, 1-61
23. Lichtenthaler, H. K. (1987) *Methods Enzymol.* **148**, 350-382
24. Giorgi, L. B., Nixon, P. J., Merry, S. A. P., Joseph, D. M., Durrant, J. R., De la Rivas, J., Barber, J., Porter, G., and Klug, D. R. (1996) *J. Biol. Chem.* **271**, 2093-2101
25. Heathcote, P., Moeenne-Loccoz, P., Rigby, S. E. J., and Evans, M. C. W. (1996) *Biochemistry* **35**, 6644-6650
26. Yang, F., Shen, G., Schluchter, W. M., Zybailov, B. L., Ganago, A. O., Vassiliev, I. R., Bryant, D. A., and Golbeck, J. H. (1998) *J. Phys. Chem. B* **102**, 8288-8299
27. Joliot, P., Beal, D., and Frilley, B. (1980) *J. Chim. Phys. Phys.-Chim. Biol.* **77**, 209-216
28. Beal, D., Rappaport, F., and Joliot, P. (1999) *Rev. Sci. Instrum.* **70**, 202-207
29. Mueller, K.-H., and Plesser, T. (1991) *Eur. Biopys. J.* **19**, 231-240
30. Diner, B. A. (1998) *Methods Enzymol.* **297**, 337-360
31. Siefermann-Harms, D. (1987) *Physiol. Plant.* **69**, 561-568

32. Britton, G., Liaaen-Jenson, S., and Pfander, H. (1995) *Carotenoids, Vol. 1B: Spectroscopy* (Britton, G., Liaaen-Jenson, S., and Pfander, H., Eds.), 1B, Birkhaeuser, Basel
33. Zeichmaster, L. (1962) *Cis-trans Isomeric Carotenoids, Vitamins A and Aryl-polyenes*, Springer, Vienna
34. Bautista, J. A., Chynwat, V., Cua, A., Jansen, F. J., Lugtenburg, J., Gosztola, D., Wasielewski, M. R., and Frank, H. A. (1998) *Photosynth. Res.* **55**, 49-65
35. Coufal, J., Hladik, J., and Sofrova, D. (1989) *Photosynthetica* **23**, 603-616
36. Britton, G. (1985) *Methods Enzymol.* **111**, 113-149
37. Zybailov, B., Van der Est, A., Zech, S. G., Teutloff, C., Johnson, T. W., Shen, G., Bittl, R., Stehlik, D., Chitnis, P. R., and Golbeck, J. H. (2000) *J. Biol. Chem.* **275**, 8531-8539
38. Van der Est, A., Prisner, T., Bittl, R., Fromme, P., Lubitz, W., Moebius, K., and Stehlik, D. (1997) *J. Phys. Chem. B* **101**, 1437-1443
39. MacMillan, F., Hanley, J., van der Weerd, L., Knuepling, M., Un, S., and Rutherford, A. W. (1997) *Biochemistry* **36**, 9297-9303
40. Romijn, J. C., and Amesz, J. (1977) *Biochim. Biophys. Acta* **461**, 327-338
41. Shen, G., Antonkine, M. L., van der Est, A., Vassiliev, I. R., Brettel, K., Bittl, R., Zech, S. G., Zhao, J., Stehlik, D., Bryant, D. A., and Golbeck, J. H. (2002) *J. Biol. Chem.* **277**, 20355-20366
42. Frank, H. A., and Cogdell, R. J. (1996) *Photochem. Photobiol.* **63**, 257-264
43. Trebst, A., and Depka, B. (1997) *FEBS Letters* **400**, 359-362
44. Brettel, K., Setif, P., and Mathis, P. (1986) *FEBS Letters* **203**, 220-224
45. Takahashi, Y., Hirota, K., and Katoh, S. (1985) *Photosynth. Res.* **6**, 183-192
46. Setif, P., and Brettel, K. (1993) *Biochemistry* **32**, 7846-7854
47. Rappaport, F., Diner, B. A., and Redding, K. (2005) in *Photosystem I: The Light-Driven Plastocyanin:Ferredoxin Oxidoreductase* (Golbeck, J. H., ed), Springer, Berlin *in press*
48. Hecks, B., Wulf, K., Breton, J., Leibl, W., and Trissl, H. W. (1994) *Biochemistry* **33**, 8619-8624
49. Muhiuddin, I. P., Heathcote, P., Carter, S., Purton, S., Rigby, S. E. J., and Evans, M. C. W. (2001) *FEBS Lett.* **503**, 56-60
50. Hashimoto, H., and Koyama, Y. (1988) *J. Phys. Chem.* **92**, 2101-2108
51. Dobek, K. and Brettel, K. (2004) in Proceedings of the 13th International Congress on Photosynthesis, Abstract 185, pp. 91
52. Ishikita, H., and Knapp, E.-W. (2003) *J. Biol. Chem.* **278**, 52002-52011
53. Van der Est, A., Valieva, A. I., Kandrashikin, Y. E., Shen, G., Bryant, D. A. and Golbeck, J. H. (2004) *Biochemistry* **43**, 1264-1275

FOOTNOTES

† The project was supported by the National Research Initiative of the USDA Cooperative State Research, Education and Extension Service, grant number 2001-35318-11270 (to B.A.D.), the National Science Foundation Grant MCB-0117079 (to J.H.G.), and the Centre National de la Recherche Scientifique and the College de France (to F.R. and M.G.-K). This paper is contribution No. 8518 of the Central Research and Development Department of the E. I. du Pont de Nemours & Co.

‡These authors contributed equally to this work. *To whom correspondence should be addressed.

We thank Dexter Chisholm for his assistance in the construction of the mutants and Boris Zybailov for his help with EPR measurements.

The abbreviations used are: A_0, primary electron acceptor; A_1, secondary electron acceptor; DCPIP, dichlorophenolindophenol; ß-DM, *n*-dodecyl-ß-D-maltoside; DCMU, 3-(3',4'-dichlorophenyl)-1,1-dimethylurea; F_x, F_A, F_B, [4Fe-4S] clusters; FCCP, carbonyl cyanide (4-(trifluoromethoxy)phenyl)hydrazone; HEPES, *N*-(2-hydroxyethyl)piperazine-*N'*-(2-ethanesulfonic acid); HPLC, high performance liquid chromatography; MES, 2-(*N*-morpholino)ethanesulfonic acid; P700, primary electron donor of PS I; PCR, Polymerase Chain Reaction; PhQ_A, phylloquinone bound by PsaA; PhQ_B, phylloquinone bound by PsaB; Pds, phytoene desaturase (encoded by *crtP* (*pds*)); PS I, Photosystem I; PS II, Photosystem II; SDS-PAGE, sodium dodecyl sulfate-polyacrylamide gel electrophoresis; Tris, tris(hydroxymethyl)aminomethane; Vit, Vitamin; WT, wild type; Zds, zeta-carotene desaturase (encoded by *crtQ* (*zds*)).

FIGURE LEGENDS

Fig 1. The biosynthetic pathway leading to ringed carotenoids in cyanobacteria starting from geranylgeranyl pyrophosphate (GGPP). The molecules are depicted in the all-*trans* configuration. The standard numbering is given in the last structure.

Fig 2. The electron transfer cofactors from the X-ray crystallographic structure of PS I from *Thermosynechococcus elongatus* at 2.5 Å resolution (*2*). The figure shows the clusters of carotenoids near the phylloquinones $PhyQ_A$ and $PhyQ_B$. The β-$carotene_{fam}$ carotenoids are color coded as follows: red – *cis*, yellow – all-*trans*. The phytyl tails of the chlorophylls have been omitted for simplicity. Note the greater number of carotenoid *cis* double bonds on the PsaA-side as compared to the PsaB-side. The coordinates of the structure were taken from the Brookhaven Protein Data Bank (entry 1JBO).

Fig 3. (a) Absorption spectra of the WT, *zds*$^-$ and *pds*$^-$ PS I complexes after normalization at the Q_y absorbance maximum. The inset shows an expansion of the region of maximum absorption of the Q_y optical transitions. (b) Subtractions of the Q_y-normalized spectra of the PS I complexes of WT minus *pds*$^-$ and of *zds*$^-$ minus *pds*$^-$, revealing the absorbance spectra of the carotenoids present in the WT and *zds*$^-$ strains.

Fig 4. HPLC chromatograms of total pigment extracts from PS I complexes of the (a) WT, (b) *zds*$^-$ and (c) *pds*$^-$ strains. The pigments were extracted and the HPLC run as described in Materials and Methods. The chromatograms were detected at 450, 400 and 288 nm, respectively, for the WT, *zds*$^-$ and *pds*$^-$ strains.

Fig 5. EPR spectra of reduced F_A and F_B in the WT, *zds*$^-$ and *pds*$^-$ PS I complexes of *Synechocystis* sp. PCC 6803. The samples were resuspended at a concentration of 1 mg Chl *a* ml^{-1} in 100 mM in glycine (pH 10) containing 50 mM in sodium dithionite. The spectra were recorded in the dark at 15 K. Spectrometer settings were as follows: microwave power, 20 mW; microwave frequency, 9.478 GHz; receiver gain, 6.3×10^4; modulation amplitude, 10 G at 100 kHz; center field, 3480 G; scan width, 1740 G. The spectra shown are the average of three scans.

Fig 6. Illuminated-minus-dark difference Q-band cw EPR spectra of A_1^- in WT, *zds*$^-$ and *pds*$^-$ PS I complexes at 205 K. The samples were suspended to a concentration of 1 mg Chl *a* ml^{-1} in Buffer A (see Materials and Methods) to which were added 100 mM glycine buffer (pH 10) and 50 mM sodium dithionite. The preillumination and post-illumination spectra were recorded as described in Materials and Methods. The instrument settings were as follows: microwave power, 1 mW; microwave frequency, 34.056 GHz; modulation frequency, 100 kHz; modulation amplitude, 1 G; time constant, 10 ms; conversion time, 10 ms; 50 scans were averaged.

Fig 7. Kinetics of A_1^- oxidation in the WT (■), *zds*$^-$ (Δ) and *pds*$^-$ (○) PS I complexes monitored at 380 nm (left) and 480 nm (right) following an actinic flash exciting 70% of the reaction centers. The PS I complexes were suspended as described in Materials and Methods.

Fig 8. Decay associated spectra from a global analysis of the relaxation kinetics of the fast (■) and slow phases (●) of the $A_1^-(FeS)$ - $A_1(FeS)^-$ in PS I complexes from the (a) WT, (b) *zds*$^-$ and (c) *pds*$^-$ strains.

Fig 9. Comparison of the *zds*$^-$ and the *pds*$^-$ decay-associated spectra with that of WT for $P700^+$ $FeS_{[A/B]}^-$ - P700 $FeS_{[A/B]}$ in PS I complexes. This spectrum was detected at 20 us following the actinic flash.

Fig 10. Fast (■) and slow phase (●) double difference spectra of the $[A_1^-(FeS) - A_1(FeS)^-]_{WT}$ - $[A_1^-(FeS) - A_1(FeS)^-]_{mutant}$ and of $[P700^+ FeS_{[A/B]}^- - P700\ FeS_{[A/B]}]_{WT}$ - $[P700^+FeS_{[A/B]}^- - P700FeS_{[A/B]}]_{mutant}$ (Δ). The spectra were normalized to the 430 nm signal of $P700^+F_{A/B}^-$ - $P700FeS_{[A/B]}$ nm measured at 20 μs such that the difference spectra were calculated at equal center concentrations.

Fig 11. Decay associated spectra in *Synechocystis* sp. 6803 whole cells of the 8 ns (■, fast phase) and 180 ns (●, slow phase) components from a global analysis of kinetic data in WT. The cells were suspended in 20 mM HEPES (pH 7.2), 20% (w/v) Ficoll, and 5 μM FCCP.

Fig 12. Charge recombination kinetics of electron transfer from $FeS_{[A/B]}^-$ to $P700^+$ monitored at 435 nm (minimum of $P700^+$- P700) after a saturating actinic flash in WT and *zds*$^-$ PS I complexes. The complexes were suspended in 25 mM Tris-HCl (pH 8.3), 10 μM sodium ascorbate, 4 μM DCPIP, and 0.03% β-DM. The chlorophyll *a* concentration for both samples was 14 μg/mL.

Fig 13. Relative reduction potentials of Photosystem I co-factors in the WT and mutant PS I complexes. Shown in the inset is a portion of the inverted region of Marcus curve.

Table 1

Strain	Carotenoids	Mole Ratio Normalized to 96 Chlorophylls
WT	β-carotene (*trans* and *cis*)	22.1
	β-cryptoxanthin/isocryptoxanthin	3.1
	zeaxanthin	0.9
zds$^-$	zeta-carotene (*trans* and central-*cis*)	10.4
	zeta-carotene (terminal *cis* or di-*cis*)	1.3
pds$^-$	phytoene	3.3

Table 2.

PS I Cores

WT		*zds*$^-$		*pds*-	
Av. 380-390 nm	480 nm	Av. 380-390 nm	480 nm	Av. 380-390 nm	480 nm
8 ns (0.24)	9 ns (0.28)	9 ns (0.22)	9 ns (0.32)	12 ns (0.20)	8 ns (0.30)
177 ns (0.76)	152 ns (0.72)	244 ns (0.78)	254 ns (0.68)	254 ns (0.80)	274 ns (0.70)

Whole cells

WT 480 nm	*zds*$^-$ 480 nm	*pds*$^-$ 480 nm
8 ns (0.39) 180 ns (0.61)	9 ns (0.40) 250ns (0.60)	6 ns (0.47) 220 ns (0.53)

Figure 1

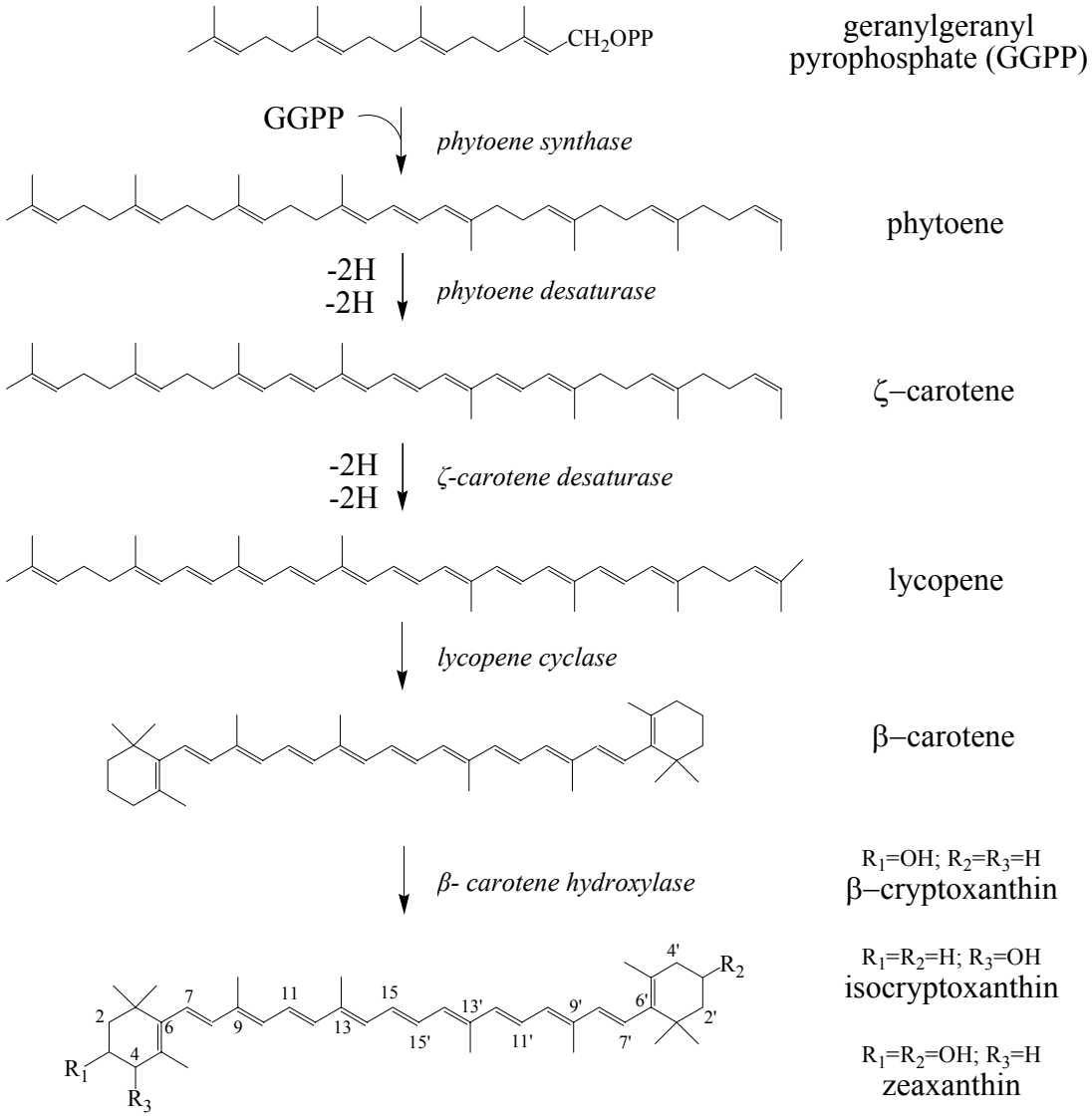
CH2OPP
geranylgeranyl pyrophosphate (GGPP)
GGPP
phytoene synthase
phytoene
-2H
-2H
phytoene desaturase
ζ–carotene
-2H
-2H
ζ-carotene desaturase
lycopene
lycopene cyclase
β–carotene
β- carotene hydroxylase
R1=OH; R2=R3=H
β–cryptoxanthin
R1=R2=H; R3=OH
isocryptoxanthin
R1=R2=OH; R3=H
zeaxanthin

Figure 2

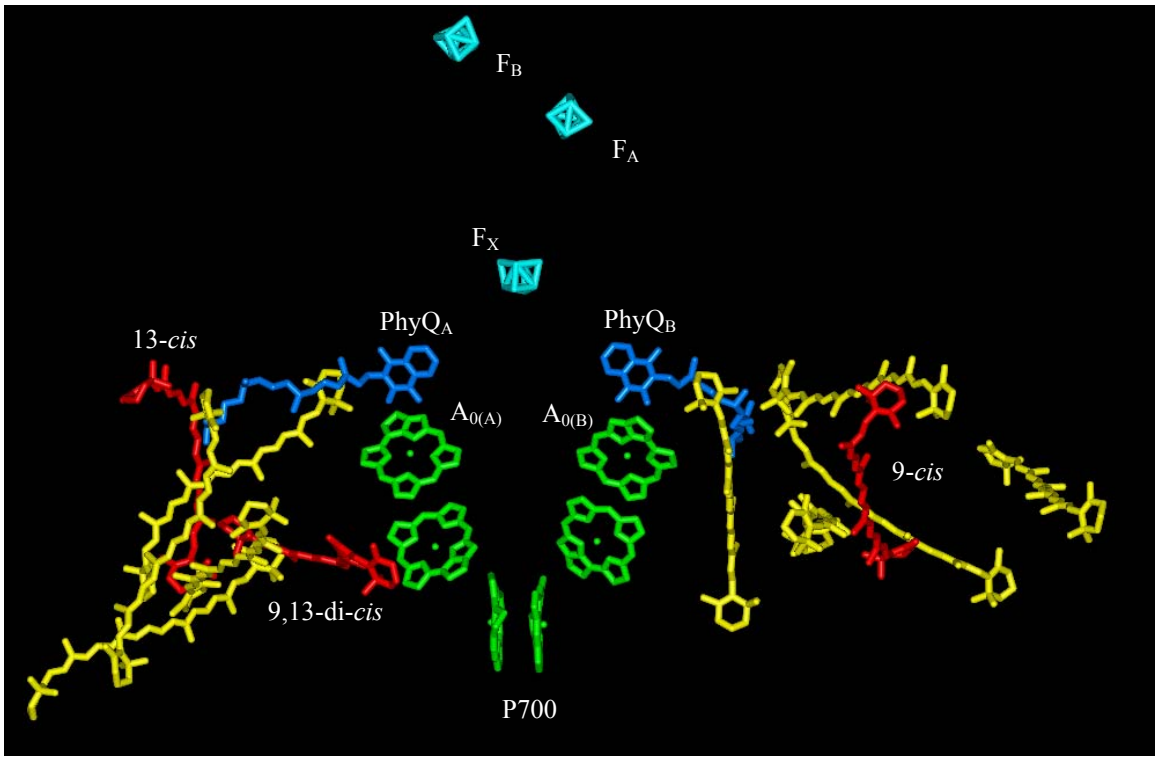

Figure 3

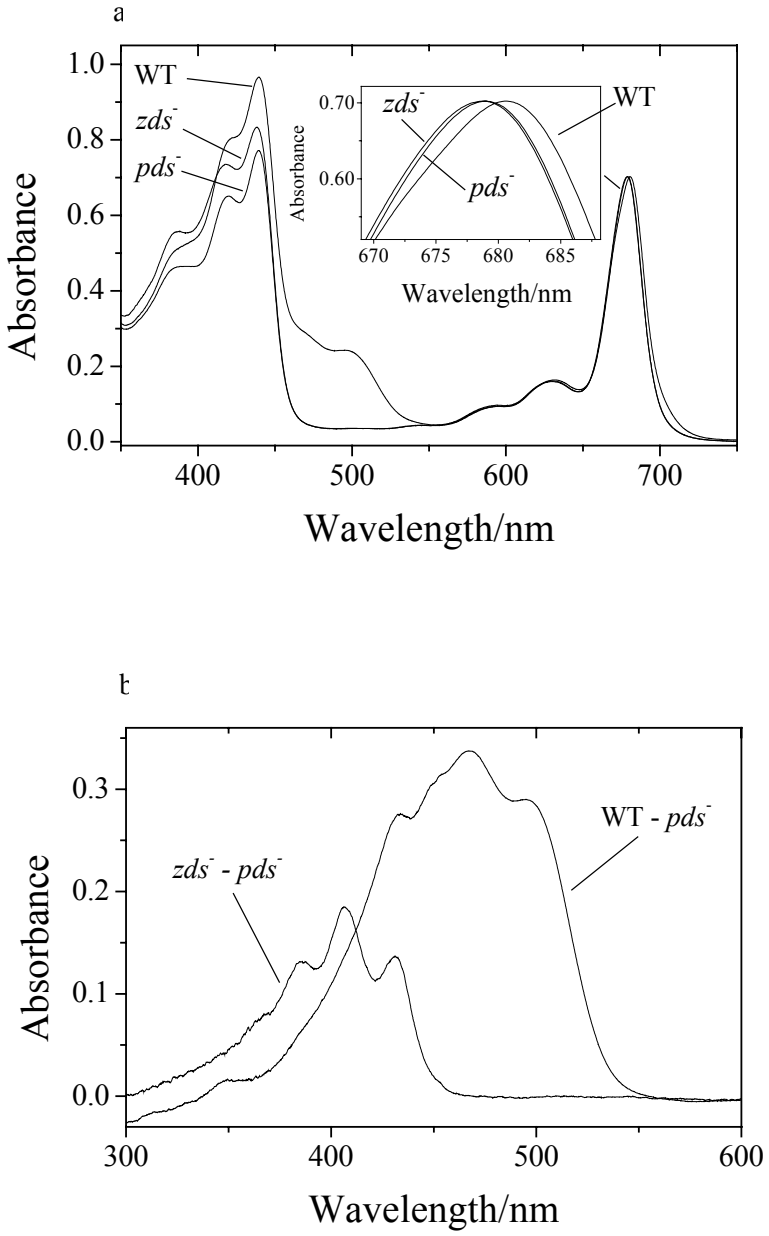
a
WT
zds-
pds-
Absorbance
Wavelength/nm
0.70
0.60
670
675
680
685
b
WT - pds-
zds- - pds-
0.3
0.2
0.1
0.0
300
400
500
600

Figure 4

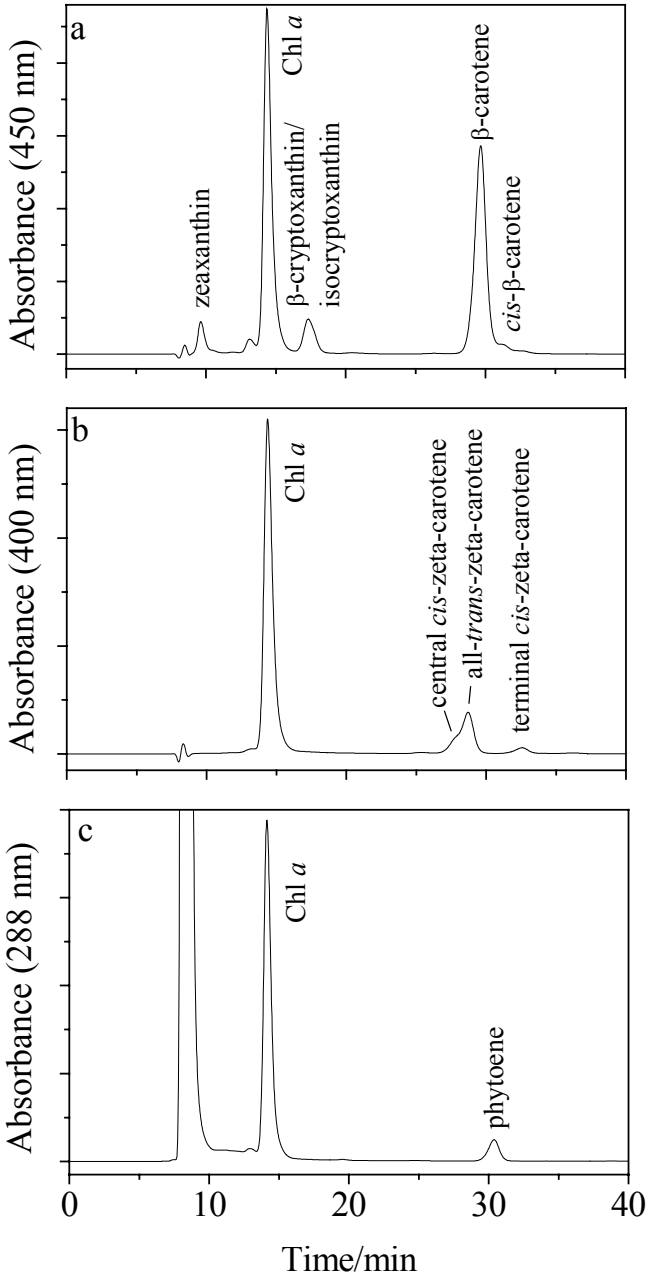
a
Absorbance (450 nm)
zeaxanthin
Chl *a*
β-cryptoxanthin/
isocryptoxanthin
β-carotene
cis-β-carotene
b
Absorbance (400 nm)
Chl *a*
central *cis*-zeta-carotene
all-*trans*-zeta-carotene
terminal *cis*-zeta-carotene
c
Absorbance (288 nm)
Chl *a*
phytoene
0
10
20
30
40
Time/min

Figure 5

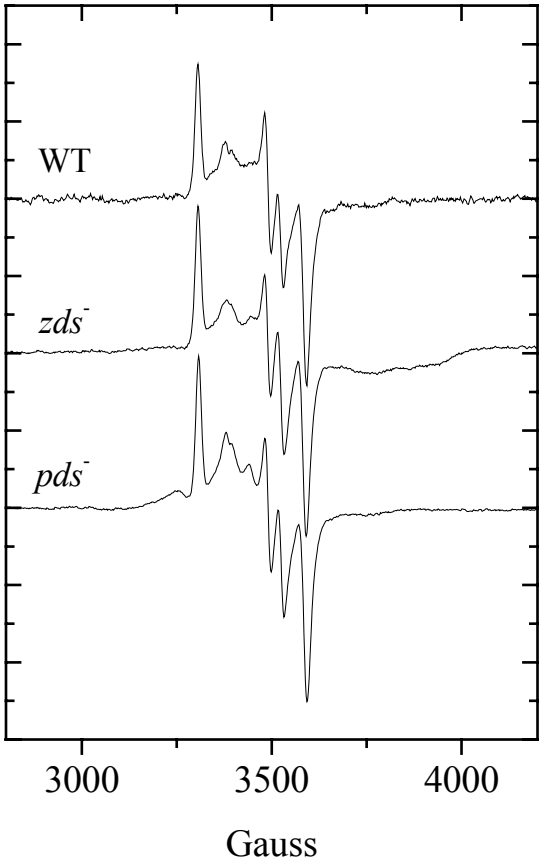

Figure 6

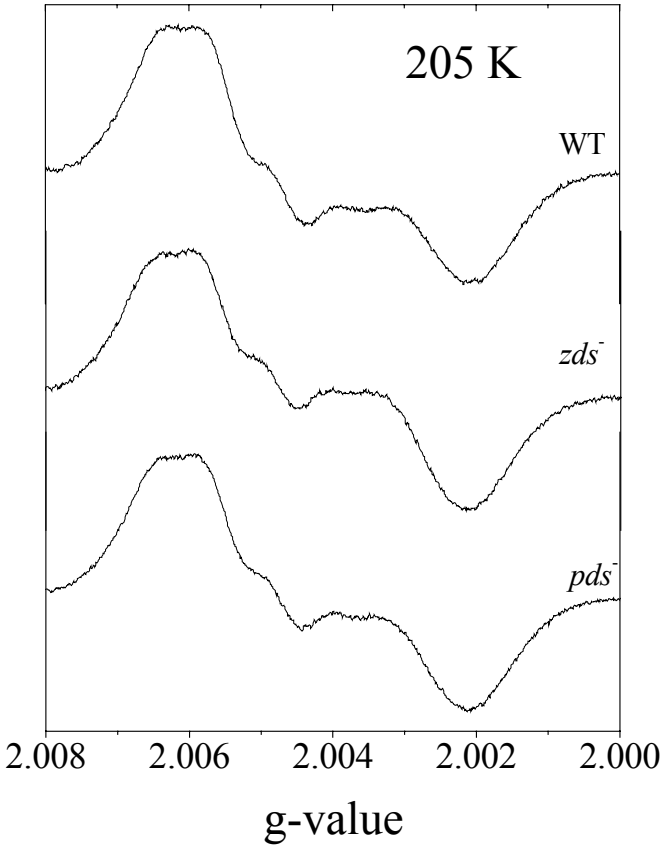

Figure 7

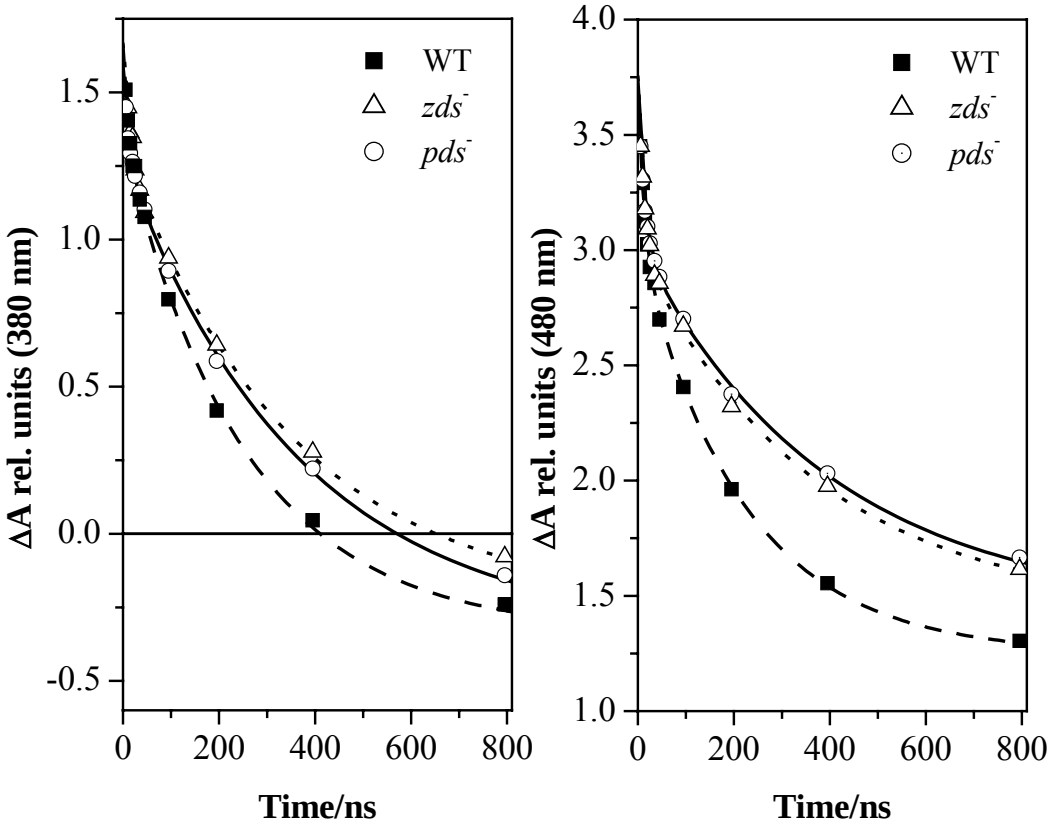
WT
zds-
pds-
ΔA rel. units (380 nm)
Time/ns
WT
zds-
pds-
ΔA rel. units (480 nm)
Time/ns

Figure 8

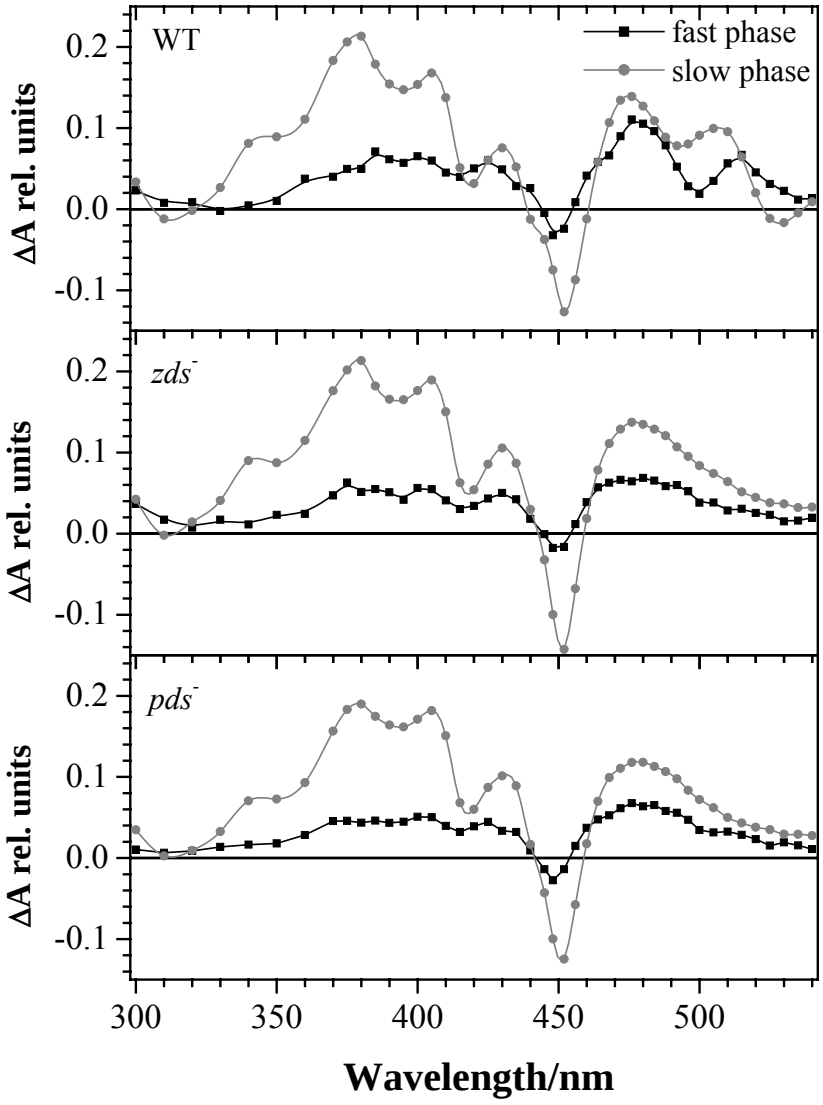
WT
fast phase
slow phase
zds-
pds-
ΔA rel. units
0.2
0.1
0.0
-0.1
300
350
400
450
500
Wavelength/nm

Figure 9

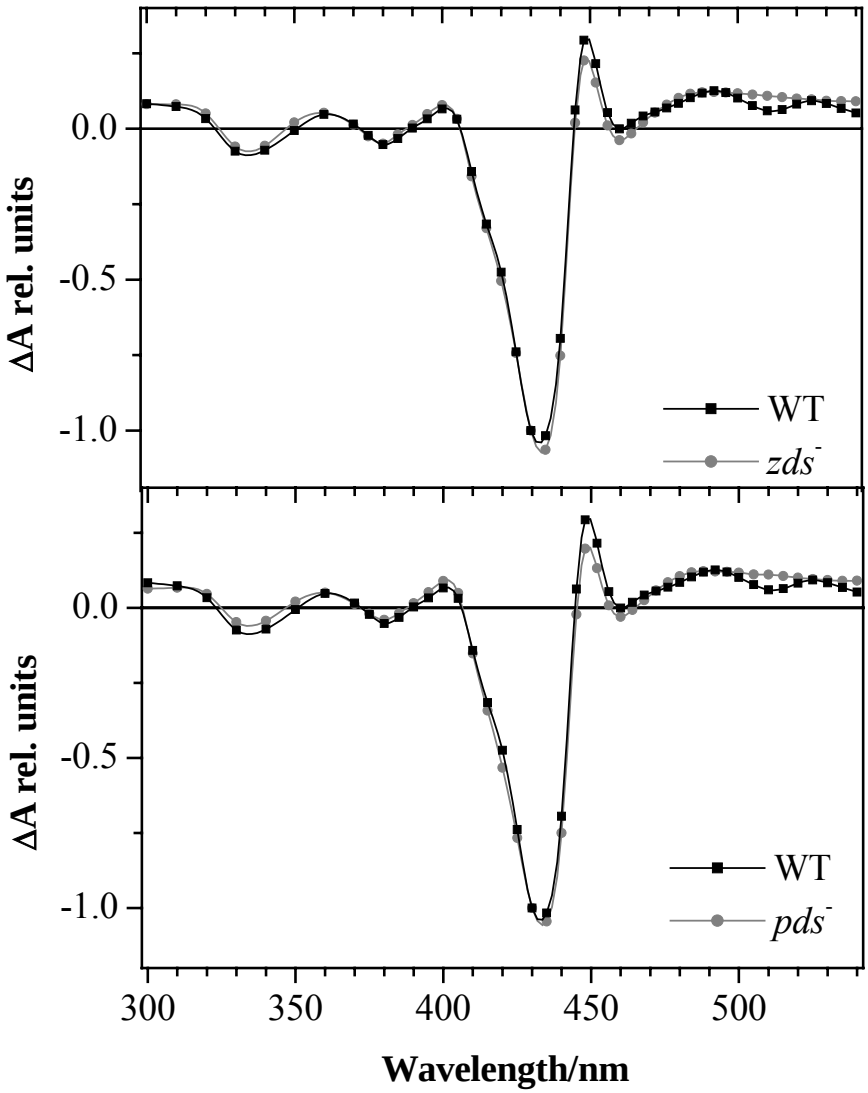
0.0
-0.5
-1.0
ΔA rel. units
WT
zds-
0.0
-0.5
-1.0
ΔA rel. units
WT
pds-
300
350
400
450
500
Wavelength/nm

Figure 10

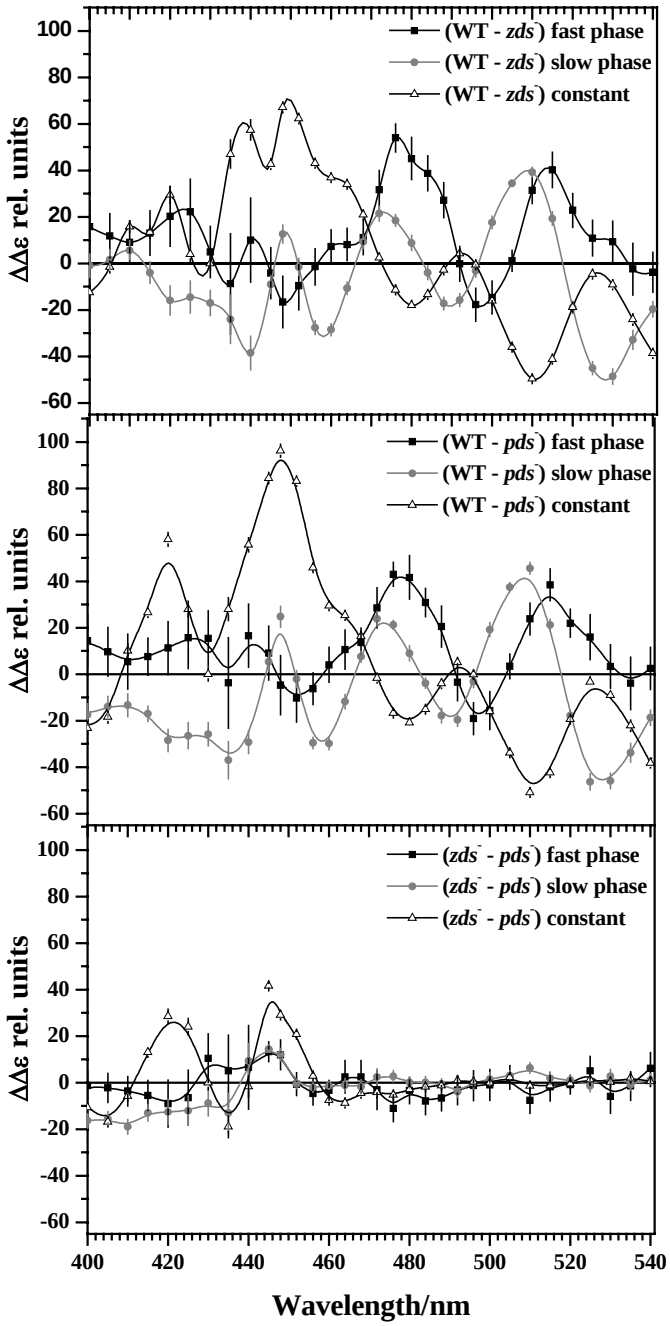
(WT - zds-) fast phase
(WT - zds-) slow phase
(WT - zds-) constant
(WT - pds-) fast phase
(WT - pds-) slow phase
(WT - pds-) constant
(zds- - pds-) fast phase
(zds- - pds-) slow phase
(zds- - pds-) constant
ΔΔε rel. units
Wavelength/nm
100
80
60
40
20
0
-20
-40
-60
400
420
440
460
480
500
520
540

Figure 11

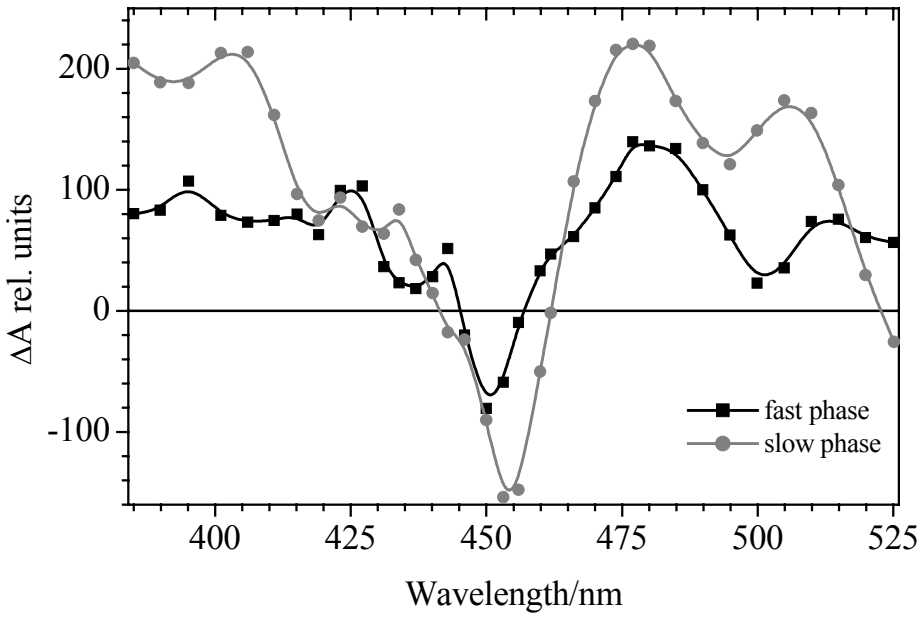
200
100
0
-100
ΔA rel. units
400
425
450
475
500
525
Wavelength/nm
fast phase
slow phase

Figure 12

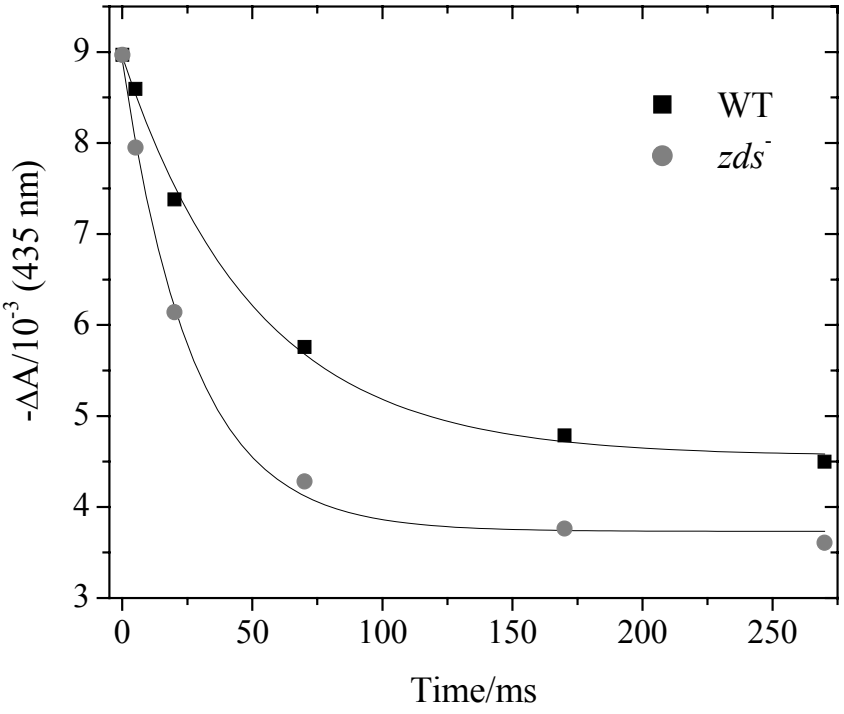

Figure 13

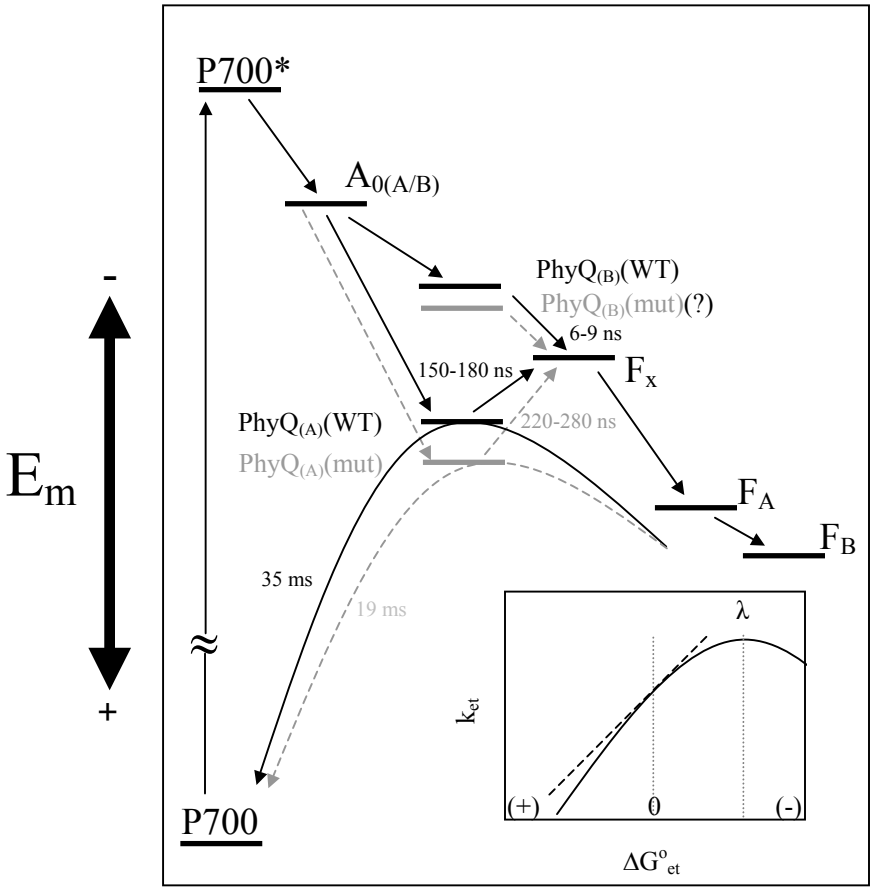
P700*
A0(A/B)
PhyQ(B)(WT)
PhyQ(B)(mut)(?)
6-9 ns
150-180 ns
Fx
PhyQ(A)(WT)
PhyQ(A)(mut)
220-280 ns
FA
FB
35 ms
19 ms
Em
-
+
≈
P700
λ
ket
(+)
0
(-)
ΔG°et